Data-driven modeling and control of large-scale dynamical systems in the Loewner framework

Methodology and Applications

Ion Victor Gosea* Charles Poussot-Vassal† Athanasios C. Antoulas‡

*Max Planck Institute for Dynamics of Complex Technical Systems, Sandtorstr. 1, 39106 Magdeburg, Germany.
Email: gosea@mpi-magdeburg.mpg.de, ORCID: 0000-0003-3580-4116
†Information Processing and Systems Department, ONERA, 2 Av. Edouard Belin, 31000, Toulouse, France.
Email: charles.poussot-vassal@onera.fr, ORCID: 0000-0001-9106-1893
‡Department of Electrical and Computer Engineering, Rice University, Houston, Texas 77005, and Max-Planck Institute for the Dynamics of Complex Technical Systems, D-39106 Magdeburg.
Email: aca@rice.edu

In this contribution, we discuss the modeling and model reduction framework known as the Loewner framework. This is a data-driven approach, applicable to large-scale systems, which was originally developed for applications to linear time-invariant systems. In recent years, this method has been extended to a number of additional more complex scenarios, including linear parametric or nonlinear dynamical systems. We will provide here an overview of the latter two, together with time-domain extensions. Additionally, the application of the Loewner framework is illustrated by a collection of practical test cases. Firstly, for data-driven complexity reduction of the underlying model, and secondly, for dealing with control applications of complex systems (in particular, with feedback controller design).

Keywords: data-driven modeling, data-driven control, Loewner matrix, rational approximation, interpolation-based methods, complex systems, feedback controller design, linear systems, parametrized systems, bilinear systems, time-domain data, time-delay systems.

1 Introduction: Data-driven modeling and control

The physical complexity of dynamical systems describing time-dependent processes stems from underlying non-linearities, the coupling dynamics, or the large amount of degrees of freedom (variables or parameters). The latter aspect is also related to enforcing specific accuracy requirements, that yield models of large dimension which are hence challenging to use for control purposes or for numerical simulations.

Simulating such complex dynamical systems is currently a common feature of many numerical software toolboxes, and is widely used both in industry and in academia. As numerical simulations become more involved, processing of increased amounts of data is required. Consequently, the number of variables under analysis is limited to the physical ones (even in the era of machine learning), while the rest are discarded. Computing simplified, easy to use dynamical models is one purpose of the model approximation and reduction discipline. Such models may then be used in a many query optimisation and simulation processes. That is why it is of critical importance to construct reliable surrogate models. Model reduction typically refers to a class of methodologies used for reducing the computational complexity of large-scale models of dynamical systems. The goal generally is to approximate the original system with a smaller and simpler system with the same structure and similar response characteristics as the original. For an overview of model reduction methods, we refer

the reader to [1, 3, 15, 16], and to the references therein. In many practical scenarios, a complete mathematical description of the dynamical system under study is not always available or not fully known. Instead of depending only on physical laws (describing partial or ordinary differential equations), one can infer important properties of the system directly from measured or computed data.

With the increasing emergence of data-driven applications in many fields of the applied sciences, the need for incorporating measurements in the modeling and controlling stage has steadily grown over the last decades. The main challenge consists in using the available data in order to effectively construct surrogate models or controllers. In this latter case, the controller has to be designed based on experimental measurements, instead of a model description. Model-based methods can hence be replaced by data-driven strategies that construct the controller, directly from experimental data. Such techniques are also known as direct methods and can be useful when control-oriented models are either too complex or too costly to obtain.

The Loewner Framework (LF) is a data-driven model identification and reduction technique that was originally introduced in [38]. It is based on the Loewner-matrix interpolation method elaborated by the third author of the current paper, more than 20 years earlier, in the seminal contribution [2]. Using only measured data, the LF constructs surrogate models directly and with low computational effort. For recent tutorial papers on LF applied to linear dynamical systems, we refer the reader to [7, 33]. Extensions that use time-domain data were provided in [11, 31] (for a Hankel matrix approach) as well as in [43] (for inferring transfer function measurements from time series). The Loewner framework has been recently extended to certain classes of nonlinear systems, such as bilinear systems in [6], and quadratic-bilinear systems in [24, 25]. An adaptive extension of the original Loewner-based method in [2], named the AAA (Adaptive-Antoulas-Anderson) algorithm, was recently proposed in [42]; it is a data-driven rational approximation method that combines interpolation and least-squares (LS) fitting.

In the first part of this contribution, the Loewner framework is mainly used as a model identification and reduction tool. In the second part, the same framework is used for feedback controller design. In the proposed setup, the reference controller is not computed by means of a given model, but using input-output data of the system. Consequently, the Loewner framework is used for synthesizing a controller directly from measured data, which shows that it is also a data-driven control tool. Data-driven control strategies consist in recasting the control design problem as an identification one. By doing so, the model simplification process is shifted directly to the controller design step. The Loewner-based data-driven control methodology was extensively studied in recent years, starting with the original contribution [35] and subsequently with [28, 45, 46, 55].
The main philosophy of the Loewner framework is as follows: starting with frequency response measurements (or, alternatively, with time-domain sequences of measured inputs and outputs), the data is arrange in a specific matrix format. Then, the dominant characteristics of the model are extracted by means of an appropriate projection (the **SVD** is the relevant tool here). Thus, simplified/reduced surrogate models can be computed without access to the specific system's description.

1.1 Notations

We denote by $\mathbb{R}$ the set of real numbers, $\mathbb{C}$ the set of complex numbers, $\mathbb{C}_+$ ($\mathbb{C}_-$) the open right (left) half plane, $\mathcal{D}$ the open unit disk, $\partial\mathcal{D}$ its boundary and $\overline{\mathcal{D}}$ the complementary of the closed unit disk, respectively. The complex variable is denoted by $\imath = \sqrt{-1}$. $\mathcal{L}_2(\mathcal{I})$ ($\mathcal{I} = \imath\mathbb{R}$ or $\partial\mathcal{D}$) denotes the set of functions that are square integrable on $\mathcal{I}$, while $\mathcal{H}_2(\mathcal{D})$ (resp. $\mathcal{H}_2(\overline{\mathcal{D}})$) is the subset of $\mathcal{L}_2(\partial\mathcal{D})$ containing the functions analytic in $\mathcal{D}$ (resp. $\overline{\mathcal{D}}$). Let $\mathcal{H}_2(\mathbb{C}_+)$, shortly $\mathcal{H}_2$, (resp. $\mathcal{H}_2(\mathbb{C}_-)$) be the subset of $\mathcal{L}_2(\imath\mathbb{R})$ containing the functions analytic in $\mathbb{C}_+$ (resp. $\mathbb{C}_-$). Similarly, $\mathcal{L}_\infty(\mathcal{I})$ ($\mathcal{I} = \imath\mathbb{R}$ or $\partial\mathcal{D}$) denotes the set of functions that are bounded on $\mathcal{I}$. $\mathcal{H}_\infty(\mathcal{D})$ (resp. $\mathcal{H}_\infty(\overline{\mathcal{D}})$) denotes the subset of $\mathcal{L}_\infty(\partial\mathcal{D})$ containing the functions analytic in $\mathcal{D}$ (resp. $\overline{\mathcal{D}}$) and $\mathcal{H}_\infty(\mathbb{C}_+)$, shortly $\mathcal{H}_\infty$, the subset of $\mathcal{L}_\infty(\imath\mathbb{R})$ of functions analytic in $\mathbb{C}_+$. The Fourier transform of a time-domain signal $v \in \mathcal{L}_2(\mathbb{R})$ is denoted by $\overline{v} = \mathcal{F}(v)$.

1.2 Organizational plan

The paper is organized as follows: after the introduction on data-driven modeling and control in Section 1, we continue with an overview on the Loewner framework for data-driven modeling in Section 2 with various

subsections that cover specific extensions of the framework. Section 3 contains three model reduction examples in the Loewner framework, while Section 4 deals with the Loewner data-driven control rationale. This illustrates how the Loewner tool can be effective for both model-based or data-driven control approaches. Finally, 5 contains the concluding remarks together with a short summary of the paper.

2 The Loewner framework for data-driven modeling: an overview

2.1 Generalities on the Loewner framework and model structures

The Loewner framework is a data-driven method aimed at building a time invariant differential algebraic equation model / realization, with associated transfer function $\mathbf{H}_{\mathcal{I}}$ or $\mathbf{H}^{(\mathcal{J})}$ (defined later). This model interpolates data obtained from experimental measurements or the evaluation of a (collection of) transfer function(s). As made clearer later in this section, according to the mathematical structure and nature of the underlying system, $\mathbf{H}_{\mathcal{I}}$ has some specific properties.

In its original form presented in [38], $\mathbf{H}^{(N)}$ ($\mathcal{J} = \{N\}$) is a descriptor linear time invariant (**LTI**) dynamical model with transfer function $\mathbf{H}^{(N)} : \mathbb{C} \to \mathbb{C}^{p\times m}$, where $N \in \mathbb{N}$ denotes the number of collected data. We also denote with $\mathbf{H}_n$ the transfer function with Mc Millan degree n ($\mathcal{I} = \{n\}$). A complete description of this case is available in the recent surveys [10, 33]. Extension to parametric **LTI** (**pLTI**) model structure also exist [32]. In this case, one obtains a multi-valued rational transfer function $\mathbf{H}^{(N,M)} : (\mathbb{C}\times\mathbb{R}) \to \mathbb{C}^{p\times m}$ where $\mathcal{J} = \{N, M\}$ data are used (or $\mathbf{H}_{r,q}$, where $\mathcal{I} = \{r, q\}$), where $M \in \mathbb{N}$ is the number of data along the parameter variable (and $q \in \mathbb{N}$ is the rational order along the parameter). The resulting rational function both interpolates the complex and real parametric variables. From a different perspective, extensions to nonlinear model structures have also been investigated. Among them, one can mention the bilinear and/or quadratic forms, explored in a series of papers [4–6, 24–26]. In these cases, the associated transfer function is a collection of multivariate coupled infinite cascade of linear systems reading as $\mathbf{H}^{(N_1)} : \mathbb{C} \to \mathbb{C}^{p\times m}$, $\mathbf{H}^{(N_1,N_2)} : (\mathbb{C}\times\mathbb{C}) \to \mathbb{C}^{p\times m}$ and $\mathbf{H}^{(N_1,N_2,\dots)} : (\mathbb{C}\times\mathbb{C}\times\dots) \to \mathbb{C}^{p\times m}$ ($\mathcal{J} = \{N_1, N_2, \dots\}$). The Loewner interpolation framework seek for function that interpolates the $N_1, N_2, \dots$ data along each related multi-valued transfer functions $\mathbf{H}^{(N_1)}$, $\mathbf{H}^{(N_1,N_2,\dots)}$ ($N_1, N_2, \dots \in \mathbb{N}$). Similarly, we denote with $\mathbf{H}_{r_1,r_2,\dots}$ the associated transfer function of order $r_1, r_2, \dots \in \mathbb{N}$.

In all the cases mentioned here, the transfer function (or the set of transfer functions) is rational, and it interpolates the data. In comparison to realization-driven model reduction, data-driven methods based on rational interpolation construct models that match the original transfer function(s) at well chosen points in the complex plane (also denoted as support points for barycentric representations [42]). As such, it provides a generalization of the Padé method to an arbitrary (set of) point(s). Data-driven methods based on rational interpolation benefits also from the fact that it only requires the transfer function evaluation, whereas projection methods require the internal model (system matrices or operators). The latter are thus referred to as *intrusive* methods, while the former are *non-intrusive* or *data-driven* ones.

In this section, an extensive review of the Loewner framework is provided, together with some of its extensions. More specifically, section 2.2 presents the Loewner framework in its original form, leading to a linear time invariant model. Extensions to linear parametric and to bilinear systems are sequentially illustrated in sections 2.3 and 2.5. As a direct extension, the time-domain Loewner, dealing with sampled time-domain data instead of frequency domain data, is covered in section 2.4.

2.2 Loewner framework in the rational LTI case

The main ingredient of the Loewner framework are summarized next in the multi-input multi-output (**MIMO**) rational **LTI** case. Let us consider that such system is a m inputs p outputs dynamical one described by a n-th order differential algebraic equation (**DAE**) model $\mathcal{S} : (\mathbf{E}, \mathbf{A}, \mathbf{B}, \mathbf{C}, \mathbf{0})$ which explicitly reads as

$$\mathcal{S} : \begin{cases} \mathbf{E}\dot{\mathbf{x}}(t) = \mathbf{A}\mathbf{x}(t) + \mathbf{B}\mathbf{u}(t)\ ,\ \mathbf{y}(t) = \mathbf{C}\mathbf{x}(t) \text{ where} \\ \mathbf{E}, \mathbf{A} \in \mathbb{R}^{n\times n}, \mathbf{B} \in \mathbb{R}^{n\times m}, \mathbf{C} \in \mathbb{R}^{p\times n}. \end{cases} \tag{1}$$

Its associated transfer function $\mathbf{H} : \mathbb{C} \longrightarrow \mathbb{C}^{p\times m}$ is

$$\mathbf{H}(\xi) = \mathbf{C}\mathbf{\Phi}(\xi)\mathbf{B} \text{ where } \mathbf{\Phi}(\xi) = (\xi\mathbf{E} - \mathbf{A})^{-1} \in \mathbb{C}^{n\times n}. \tag{2}$$

Importantly, as any rational function, relation (2) can be characterized in its Lagrangian basis with distinct Lagrange nodes (or support points) $\lambda_i \in \mathbb{C}$. Then one can rewrite it in its rational barycentric formula as follows (for $\alpha_i \neq 0$),

$$\mathbf{H}(\xi) = \frac{\sum_{i=1}^{n+1} \beta_i \mathbf{q}_i(\xi)}{\sum_{i=1}^{n+1} \alpha_i \mathbf{q}_i(\xi)} \text{ where } \mathbf{q}_i(\xi) = \frac{1}{\xi - \lambda_i}. \tag{3}$$

Let this system generate the right (or column) data together with the left (or row) data, as follows

$$\left.\begin{array}{c}(\lambda_i, \mathbf{r}_i, \mathbf{w}_i)\\ \text{for } i = 1, \ldots, \overline{n}\end{array}\right\} \text{ and } \left\{\begin{array}{c}(\mu_j, \mathbf{l}_j^T, \mathbf{v}_j^T)\\ \text{for } j = 1, \ldots, \underline{n}\end{array}\right., \tag{4}$$

where $\mathbf{w}_i = \mathbf{H}(\lambda_i)\mathbf{r}_i$ and $\mathbf{v}_j^T = \mathbf{l}_j^T\mathbf{H}(\mu_j)$, with $\mathbf{r}_i \in \mathbb{C}^{m\times 1}$, $\mathbf{l}_j \in \mathbb{C}^{p\times 1}$, $\mathbf{w}_i \in \mathbb{C}^{p\times 1}$ and $\mathbf{v}_j \in \mathbb{C}^{m\times 1}$ $(m, p \geq 1)$. In addition, we define the set of distinct interpolation points $\{z_k\}_{k=1}^N \subset \mathbb{C}$, leading to responses $\{\Phi_k\}_{k=1}^N \in \mathbb{C}^{p\times m}$, rearranged as follows $(N = \overline{n} + \underline{n})$,

$$\{z_k\}_{k=1}^N = \{\lambda_i\}_{i=1}^{\overline{n}} \cup \{\mu_j\}_{j=1}^{\underline{n}} \text{ and } \{\Phi_k\}_{k=1}^N = \{\mathbf{w}_i\}_{i=1}^{\overline{n}} \cup \{\mathbf{v}_j\}_{j=1}^{\underline{n}}. \tag{5}$$

The method then consists in building the *Loewner* matrix $\mathbb{L} \in \mathbb{C}^{\underline{n}\times\overline{n}}$ and *shifted Loewner* matrix $\mathbb{M} \in \mathbb{C}^{\underline{n}\times\overline{n}}$ defined as follows, for $i = 1, \ldots, \overline{n}$ and $j = 1, \ldots, \underline{n}$:

$$\begin{array}{rcccl}\mathbb{L}_{(j,i)} & = & \dfrac{\mathbf{v}_j^T\mathbf{r}_i - \mathbf{l}_j^T\mathbf{w}_i}{\mu_j - \lambda_i} & = & \dfrac{\mathbf{l}_j^T\left(\mathbf{H}(\mu_j) - \mathbf{H}(\lambda_i)\right)\mathbf{r}_i}{\mu_j - \lambda_i},\\ \mathbb{M}_{(j,i)} & = & \dfrac{\mu_j\mathbf{v}_j^T\mathbf{r}_i - \lambda_i\mathbf{l}_j^T\mathbf{w}_i}{\mu_j - \lambda_i} & = & \dfrac{\mathbf{l}_j^T\left(\mu_j\mathbf{H}(\mu_j) - \lambda_i\mathbf{H}(\lambda_i)\right)\mathbf{r}_i}{\mu_j - \lambda_i}.\end{array} \tag{6}$$

Additionally, let $\mathbb{W} = [\mathbf{w}_1, \cdots, \mathbf{w}_{\overline{n}}]$ and $\mathbb{V} = [\mathbf{v}_1, \cdots, \mathbf{v}_{\underline{n}}]^T$. Finally, let $\mathbf{\Lambda} = \text{diag}\,(\lambda_1, \cdots, \lambda_{\overline{n}})$, $\mathbf{M} = \text{diag}\,(\mu_1, \cdots, \mu_{\underline{n}})$, $\mathbf{R} = [\mathbf{r}_1, \cdots, \mathbf{r}_{\overline{n}}]$ and $\mathbf{L} = [\mathbf{l}_1, \cdots, \mathbf{l}_{\underline{n}}]$. The following Sylvester equations are hence satisfied by the Loewner $\mathbb{L}$ and shifted Loewner $\mathbb{M}$ matrices:

$$\mathbf{M}\mathbb{L} - \mathbb{L}\mathbf{\Lambda} = \mathbb{V}\mathbf{R} - \mathbf{L}\mathbb{W} \text{ and } \mathbf{M}\mathbb{M} - \mathbb{M}\mathbf{\Lambda} = \mathbf{M}\mathbb{V}\mathbf{R} - \mathbf{L}\mathbb{W}\mathbf{\Lambda}. \tag{7}$$

Then, the descriptor realization[1],

$$\mathcal{S}^{(N)} : \left\{\begin{array}{l}\mathbf{E}^{(N)}\dot{\mathbf{x}}(t) = \mathbf{A}^{(N)}\mathbf{x}(t) + \mathbf{B}^{(N)}\mathbf{u}(t)\ ,\ \mathbf{y}(t) = \mathbf{C}^{(N)}\mathbf{x}(t) \text{ where },\\ \mathbf{E}^{(N)}, \mathbf{A}^{(N)} \in \mathbb{C}^{\underline{n}\times\overline{n}}, \mathbf{B}^{(N)} \in \mathbb{C}^{\underline{n}\times m}, \mathbf{C}^{(N)} \in \mathbb{C}^{p\times\overline{n}}.\end{array}\right. \tag{8}$$

where $\mathbf{E}^{(N)} = -\mathbb{L}$, $\mathbf{A}^{(N)} = -\mathbb{M}$, $\mathbf{B}^{(N)} = \mathbb{V}$ and $\mathbf{C}^{(N)} = \mathbb{W}$ and which associated transfer function $\mathbf{H}^{(N)} : \mathbb{C} \longrightarrow \mathbb{C}^{p\times m}$

$$\mathbf{H}^{(N)}(\xi) = \mathbf{C}^{(N)}\mathbf{\Phi}^{(N)}(\xi)\mathbf{B}^{(N)} \text{ where } \mathbf{\Phi}^{(N)}(\xi) = (\xi\mathbf{E}^{(N)} - \mathbf{A}^{(N)})^{-1} \in \mathbb{C}^{\underline{n}\times\overline{n}} \tag{9}$$

tangentially interpolates $\mathbf{H}$ at the given support points and directions defined in (4), *i.e.* satisfies the conditions

$$\mathbf{H}^{(N)}(\lambda_i)\mathbf{r}_i = \mathbf{H}(\lambda_i)\mathbf{r}_i \text{ and } \mathbf{l}_j^T\mathbf{H}^{(N)}(\mu_j) = \mathbf{l}_j^T\mathbf{H}(\mu_j). \tag{10}$$

Note that $\mathbf{H}^{(N)}$ or $\mathcal{S}^{(N)}$ is an interpolant of the data without any reduction. It refers to the realization constructed using the N available data.

From now on, let us assume that $\underline{n} = \overline{n}$, also referred to as the square case[2]. Moreover, assuming that the number $N = \underline{n} + \overline{n}$ of available data is large enough, then it was shown in [38] that a minimal model $\mathbf{H}_r$

[1] Note here that the capital subscript N denotes the number of considered data.

[2] The term square refers to the square shape of the dynamic matrices $\mathbf{A}$ and $\mathbf{E}$. More details can be found in [8].

of dimension $r < \overline{n} = \underline{n}$ still satisfying the interpolatory conditions (10) can be computed by projecting the realization (8), provided that the following holds (for $k = 1, \ldots, N$)[3]

$$\mathbf{rank}(z_k\mathbb{L} - \mathbb{M}) = \mathbf{rank}([\mathbb{L}, \mathbb{M}]) = \mathbf{rank}([\mathbb{L}^H, \mathbb{M}^H]^H) = r, \tag{11}$$

where z_k are as in (5). Let $\mathbf{Y} \in \mathbb{C}^{\underline{n} \times r}$ (resp. $\mathbf{X} \in \mathbb{C}^{\overline{n} \times r}$) be the matrix containing the first r left (resp. right) singular vectors of $[\mathbb{L}, \mathbb{M}]$ (resp. $[\mathbb{L}^H, \mathbb{M}^H]^H$). Then, $\mathcal{S}_r : (\mathbf{E}_r, \mathbf{A}_r, \mathbf{B}_r, \mathbf{C}_r, \mathbf{0})$ where

$$\mathbf{E}_r = \mathbf{Y}^H\mathbf{E}^{(N)}\mathbf{X}\ ,\ \mathbf{A}_r = \mathbf{Y}^H\mathbf{A}^{(N)}\mathbf{X}\ ,\ \mathbf{B}_r = \mathbf{Y}^H\mathbf{B}^{(N)} \text{ and } \mathbf{C}_r = \mathbf{C}^{(N)}\mathbf{X}, \tag{12}$$

is a descriptor realization of $\mathbf{H}_r$, given as

$$\mathbf{H}_r(\xi) = \mathbf{C}_r\mathbf{\Phi}_r(\xi)\mathbf{B}_r \text{ where } \mathbf{\Phi}_r(\xi) = (\xi\mathbf{E}_r - \mathbf{A}_r)^{-1} \in \mathbb{C}^{r \times r}, \tag{13}$$

encoding a *minimal Mc Millan degree* equal to $\nu = \mathbf{rank}(\mathbb{L})$. Note that if r in (11) is greater than $\mathbf{rank}(\mathbb{L})$, then $\mathbf{H}_r$ may either have a direct feed-through term or a polynomial part. Finally, the number r of singular vectors composing $\mathbf{Y}$ and $\mathbf{X}$ used to project the system $\mathbf{H}_r$ in (12) may be decreased to at the cost of imposing an approximate interpolation of data, leading to the reduced order rational model. This allows a trade-off between complexity of the resulting model and accuracy of the interpolation. The Loewner framework thus is a landmark appropriate for identification, approximation and order reduction.

Let us close this first part with two linear differential algebraic equations examples where the Loewner framework is applied. Both continuous and sampled-time cases are considered, highlighting how versatile this landmark is. More detailed and didactic examples may be found in the surveys [10, 33].

Example 1 (Continuous-time rational and polynomial model interpolation) *Let us consider the following rational and polynomial (improper) model,* $\mathbf{H}(s) = s + 1/(s+1) = (s^2 + s + 1)/(s+1)$ *which a realization* $\mathcal{S} : (\mathbf{E}, \mathbf{A}, \mathbf{B}, \mathbf{C}, \mathbf{0})$ *can be described as follows:*

$$\mathbf{E} = \begin{bmatrix} 0 & 1 & 0 \\ 0 & 0 & 1 \\ 0 & 0 & 1 \end{bmatrix}, \mathbf{A} = \begin{bmatrix} 1 & 0 & 0 \\ 0 & 1 & 0 \\ 0 & 0 & -1 \end{bmatrix}, \mathbf{B} = \begin{bmatrix} 0 \\ 0 \\ 1 \end{bmatrix} \text{ and } \mathbf{C}^T = \begin{bmatrix} 1 \\ 1 \\ 1 \end{bmatrix}. \tag{14}$$

By sampling $\mathbf{H}$ *with the following support points* $\lambda_i = \{1, 3, 5, 7\}$ *and* $\mu_j = \{2, 4, 6, 8\}$ *and tangential directions* $\mathbf{r}_i = \mathbf{l}_j = 1$ *for* $i, j = 1, \ldots, 4 = \overline{n} = \underline{n}$ *(*$N = 8$*), leads to the measurements* $\mathbf{w}_i = \{3/2, 13/4, 31/6, 57/8\}$ *and* $\mathbf{v}_j = \{7/3, 21/5, 43/7, 73/9\}$. *Constructing the Loewner matrices as in (6), one obtains a 4-th order realization* $\mathcal{S}_N : (-\mathbb{L}, -\mathbb{M}, \mathbb{V}, \mathbb{W})$. *Following (11), the rank of the* $[\mathbb{L}, \mathbb{M}]$ *matrix is equal to* $r = 3$. *Practically, by computing the* ***SVD*** *of the* $[\mathbb{L}, \mathbb{M}]$ *matrix leads to the following normalized singular values* $\sigma = \{1, 5.59 \cdot 10^{-2}, 6.8804 \cdot 10^{-4}, 5.8311 \cdot 10^{-17}\}$ *and thus suggests to preserve the* $r = 3$ *first columns of* $\mathbf{Y}$ *and* $\mathbf{X}$*, as in (12). After projection, this leads to a minimal order realization which related transfer function exactly recovers the original* $\mathbf{H}$ *one, with Mc Millan degree of* $\nu = 2$ *and associated realization* $r = 3$. *In addition, computing the singularities of the associated pencil* $(\mathbb{M}, \mathbb{L})$ *gives* $\{-1, \infty, \infty\}$*, being exactly the one of the original model* $\mathbf{H}$. *The singularity in* -1 *is related to the rational part of* $\mathbf{H}$*,* $1/(s+1)$*, being the finite dynamic mode. Then, the two singularities in* ∞ *are related to the impulsive (irrational part) and non-dynamic (direct feed-through term) modes.*

Example 2 (Interpolation in the sampled-time) *Let us now consider the discrete-time model* $\mathbf{H}(z) = z/(z - 1/2)$*, sampled with a constant period* $h = 1$ *second. One may evaluate the function on the unit circle centered in zero, being the projection of the imaginary axis classically considered in continuous-time. Then, by choosing* $\lambda_i = \{e^{-\imath 0.1h}, e^{\imath 0.1h}, e^{-\imath 2h}, e^{\imath 2h}\}$*,* $\mu_j = \{e^{-\imath h}, e^{\imath h}, e^{-\imath 3h}, e^{\imath 3h}\}$ *and tangential directions* $\mathbf{r}_i = \mathbf{l}_j = 1$ *for* $i, j = 1, \ldots, 4 = \overline{n} = \underline{n}$ *(*$N = 8$*), one respectively obtains* $\mathbf{w}_i$ *and* $\mathbf{v}_j$ *(notice that the Nyquist pulsation, being the maximal pulsation prior periodic frequency response is at* $\omega_N = \pi/h$ *rad/s). By construction, the Loewner*

[3] Note here that the lower subscript letter r denotes the dimension of the realization instead of the number of data (in the capital case).

matrices are complex of dimension 4×4. *As data are provided in complex conjugate form, one may work with real arithmetic instead of complex ones by projecting the data (see §2.5.4 [33] for details). Then, one obtains*

$$\begin{array}{rcl} \mathbf{\Lambda} & = & \textbf{\textit{blkdiag}}\left(\left[\begin{array}{cc} 0.9950 & -0.0998 \\ 0.0998 & 0.9950 \end{array} \right], \left[\begin{array}{cc} -0.4161 & -0.9093 \\ 0.9093 & -0.4161 \end{array} \right] \right), \\ \mathbf{R} & = & [\sqrt{2}, 0, \sqrt{2}, 0]\ , \\ \mathbf{W} & = & [2.7869, 0.2768, 1.0254, 0.3859] \\ \mathbf{M} & = & \textbf{\textit{blkdiag}}\left(\left[\begin{array}{cc} 0.5403 & -0.8415 \\ 0.8415 & 0.5403 \end{array} \right], \left[\begin{array}{cc} -0.9900 & -0.1411 \\ 0.1411 & -0.9900 \end{array} \right] \right), \\ \mathbf{L} & = & [\sqrt{2}, 0, \sqrt{2}, 0]^T \textit{ and} \\ \mathbf{V} & = & [1.4544, -0.8384, 0.9439, -0.0445]^T\ , \end{array} \tag{15}$$

By then solving (7)*, one readily obtains* $\mathbb{L}$ *and* $\mathbb{M}$ *and the associated 4-th order realization* $\mathcal{S}_N : (-\mathbb{L}, -\mathbb{M}, \mathbf{V}, \mathbf{W}, \mathbf{0})$. *Applying the rank revealing factorisation* (11) *and* (12)*, one obtains the Mc Millan degree* $\nu = \textbf{\textit{rank}}(\mathbb{L}) = 1$ *and* $r = 2$. *This indicates a constant term. By applying the procedure detailed in [29], one may reconstruct the direct term by the infinite eigenvalue computation of the* $(\mathbb{M}, \mathbb{L})$ *pencil (or zero eigenvalue of* $(\mathbb{L}, \mathbb{M})$*). In this case one finds* $D = 1$. *By removing it from the raw data and re-compute the Loewner procedure one gets* $\nu = r = 1$ *and the sampled realization* $(\mathbf{E}_1, \mathbf{A}_1, \mathbf{B}_1, \mathbf{C}_1, \mathbf{D}_1) = (2.897, 1.448, -0.9632, -1.504, 1)$*, which transfer function* $\mathbf{H}_1 = (z - 1.665 \times 10^{-16})/(z - 0.5)$*, recovering almost perfectly the original model* $\mathbf{H}$. *Note that in this case, the realization is a sampled one and time-domain dynamical equation reads* $\mathbf{E}_1\mathbf{x}(t_{k+1}) = \mathbf{A}_1\mathbf{x}(t_k) + \mathbf{B}_1\mathbf{u}(t_k)$ *and* $\mathbf{y}(t_k) = \mathbf{C}_1\mathbf{x}(t_k) + \mathbf{D}_1\mathbf{u}(t_k)$*, where* $t_{k+1} = t + kh$.

2.3 Generalizations to parametric linear systems

The Loewner framework has been extended to parametric **LTI** (**pLTI**) systems, first in [9] and in a more detailed manner in [32][4]. In parametric model approximation and reduction, the aim is to construct reduced-order models that match the response of the original model / data, along the dynamical parameter ξ (usually complex) and along the parameters ρ (traditionally real). In what follows we will only show how the two variable case works, *i.e.* with one single parameter $\rho \in \mathbb{R}$ (for further extensions, see [32]). We construct models which are reduced both with respect to the complex variable (or frequency) and to the real one (parameter). In this configuration let us consider such a m input p output ρ-parametrized dynamical system described by a n-th order differential algebraic equation (**DAE**) model denoted $\mathcal{S}(\rho) : (\mathbf{E}(\rho), \mathbf{A}(\rho), \mathbf{B}(\rho), \mathbf{C}(\rho), \mathbf{0})$ given as

$$\mathcal{S}(\rho) : \left\{ \begin{array}{l} \mathbf{E}(\rho)\dot{\mathbf{x}}(t) = \mathbf{A}(\rho)\mathbf{x}(t) + \mathbf{B}(\rho)\mathbf{u}(t)\ ,\ \mathbf{y}(t) = \mathbf{C}(\rho)\mathbf{x}(t) \text{ where} \\ \mathbf{E}(\rho), \mathbf{A}(\rho) \in \mathbb{R}^{n\times n}, \mathbf{B}(\rho) \in \mathbb{R}^{n\times m}, \mathbf{C}(\rho) \in \mathbb{R}^{p\times n}, \rho \in \mathbb{R}. \end{array} \right. \tag{16}$$

with associated transfer function $\mathbf{H} : (\mathbb{C} \times \mathbb{R}) \rightarrow \mathbb{C}^{p\times m}$

$$\mathbf{H}(\xi, \rho) = \mathbf{C}(\rho)\mathbf{\Phi}(\xi, \rho)\mathbf{B}(\rho) \text{ where } \mathbf{\Phi}(\xi, \rho) = (\xi\mathbf{E}(\rho) - \mathbf{A}(\rho))^{-1} \in \mathbb{C}^{n\times n}. \tag{17}$$

As for the Loewner case, let us assume that function (17) can be expressed in the Lagrange, using the distinct Lagrange support points λ_i and π_j, as (for $\alpha_{ij} \neq 0$)

$$\mathbf{H}(\xi, \rho) = \frac{\sum_{i=1}^{n+1}\sum_{j}^{m+1} \beta_{ij}\mathbf{q}_{ij}(\xi, p)}{\sum_{i=1}^{n+1}\sum_{j=1}^{m+1} \alpha_{ij}\mathbf{q}_{ij}(\xi, p)} \text{ where } \mathbf{q}_{ij}(\xi, p) = \frac{1}{(\xi - \lambda_i)(\rho - \pi_j)}. \tag{18}$$

Computation of the approximant is done in a similar way as for the non-parametric rational case: one seeks the β_{ij} and α_{ij} of the rational barycentric formula (18). Let us assume that the system $\mathbf{H}(\xi, \rho)$ is sampled along the dynamical parameter ξ and the parametric one ρ as follows

$$\{z_k\}_{k=1}^{N} = \{\lambda_i\}_{i=1}^{\overline{n}} \cup \{\mu_j\}_{j=1}^{\underline{n}} \text{ and } \{p_l\}_{l=1}^{M} = \{\pi_i\}_{i=1}^{\overline{m}} \cup \{\nu_j\}_{j=1}^{\underline{m}}. \tag{19}$$

[4]The approach developed in [32] interpolates more combinations of frequencies and parameter than the one in [9], which interpolates an extended Loewner matrix, leading to the coefficients of rational function given in Barycentric form.

Each $k = 1, \ldots, N$ and $l = 1, \ldots, M$ provides $\mathbf{H}(z_k, p_l) = \Phi_{k,l}$. Thus the measurement matrix reads

$$\Phi = \begin{bmatrix} \Phi_{(11)} & \Phi_{(12)} \\ \Phi_{(21)} & \Phi_{(22)} \end{bmatrix} \in \mathbb{C}^{N \times M}, \tag{20}$$

where $\Phi_{(11)} = \Phi_{1,\ldots,\overline{n}/1,\ldots,\overline{m}} \in \mathbb{C}^{\overline{n} \times \overline{m}}$, $\Phi_{(12)} = \Phi_{1,\ldots,\overline{n}/1,\ldots,\underline{m}} \in \mathbb{C}^{\overline{n} \times \underline{m}}$, $\Phi_{(21)} = \Phi_{1,\ldots,\underline{n}/1,\ldots,\overline{m}} \in \mathbb{C}^{\underline{n} \times \overline{m}}$ and $\Phi_{(22)} = \Phi_{1,\ldots,\underline{n}/1,\ldots,\underline{m}} \in \mathbb{C}^{\underline{n} \times \underline{m}}$. The rows correspond to frozen values of z_k related to the dynamical (complex) ξ parameter. The columns correspond to frozen p_l values related to the (real) ρ parameter. Similarly to the non-parametric case mentioned in section 2.2, one may construct the following one variable Loewner matrices

$$\begin{array}{ll} \mathbb{L}_2 \in \mathbb{C}^{\underline{nm} \times \overline{nm}} & \text{associated to } \Phi_{(11)} \text{ along } \lambda_i \bigcup \pi_j \\ \mathbb{L}_{\lambda_i} \in \mathbb{C}^{\underline{m} \times \overline{m}} & \text{associated to the } i\text{-th row of } [\Phi_{(11)}, \Phi_{(12)}] \text{ along } p_l \\ \mathbb{L}_{\pi_j} \in \mathbb{C}^{\underline{n} \times \overline{n}} & \text{associated to the } j\text{-th column of } [\Phi_{(11)}^H, \Phi_{(21)}^H]^H \text{ along } z_k \end{array} \tag{21}$$

and the global two dimensional Loewner matrix $\widehat{\mathbb{L}_2} \in \mathbb{C}^{(\overline{n}\underline{m}+\underline{n}\overline{m}+\underline{nm}) \times (\overline{nm})}$

$$\widehat{\mathbb{L}_2} = \begin{bmatrix} \mathbb{L}_\lambda \\ \mathbb{L}_\pi \\ \mathbb{L}_2 \end{bmatrix}, \text{ where } \mathbb{L}_\lambda = \begin{bmatrix} \mathbf{e}_1^T \otimes \mathbb{L}_{\lambda_1} \\ \vdots \\ \mathbf{e}_{\overline{n}}^T \otimes \mathbb{L}_{\lambda_{\overline{n}}} \end{bmatrix} \text{ and } \mathbb{L}_\pi = \begin{bmatrix} \mathbb{L}_{\pi_1} \otimes \mathbf{e}_1^T \\ \vdots \\ \mathbb{L}_{\pi_{\overline{n}}} \otimes \mathbf{e}_{\overline{m}}^T \end{bmatrix}. \tag{22}$$

As in the non-parametric case, one important step is the determination of the minimal rational orders n and m in (18) hidden in the data collection. Here again, this is computed by a rank revealing operation, namely evaluating the null-space of the single variable Loewner matrices combinations

$$r = \max_l \mathbf{rank}\, \mathbb{L}_{p_l} \text{ and } q = \max_k \mathbf{rank}\, \mathbb{L}_{z_k}, \tag{23}$$

where $\mathbb{L}_{p_l}$ and $\mathbb{L}_{z_k}$ are the one dimensional Loewner matrices associated to the k-th row and l-th column of Φ, respectively. Then, one can simply set

$$(\overline{n}, \overline{m}) = (r + 1, q + 1), \tag{24}$$

and partition the data (19)-(20), and reconstruct (22). The two dimensional Lowner matrices ensure $\mathbf{rank}\, \widehat{\mathbb{L}_2} = \mathbf{rank}\, \mathbb{L}_2 = \overline{nm} - (\overline{n} - r)(\overline{m} - q) = \overline{nm} - 1$. The coefficients α_{ij} and β_{ij} of the rational two variables barycentric function interpolating the data, are obtained by computing the null-space of $\widehat{\mathbb{L}_2}$ as

$$\mathbf{c} = \mathbf{ker}\, \widehat{\mathbb{L}_2} \text{ where } \mathbf{c} \in \mathbb{C}^{(r+1) \times (q+1)} \tag{25}$$

Note that it is usually preferred to work with real arithmetic, *e.g.* for model time domain simulation or control design and analysis. In that case z_k are compiled in a closed conjugate form and support points are doubled (refer to §A.2 of [32] for detailed exposition). Note also that a trade-off between accuracy and complexity with both the frequency and the parameter variables can be obtained by decreasing the order r and q below the one given by (23).

Following the barycentric formulae, as exposed in [32] and [9], one may reconstruct the associated multi-valued transfer function $\mathbf{H}_{r,q} : (\mathbb{C} \times \mathbb{R}) \rightarrow \mathbb{C}^{p \times m}$ as follows (where $N_{r,q} = r + 2q + 2$ and $\mathbf{\Phi}(\xi, \rho) \in \mathbb{C}^{N_{r,q} \times N_{r,q}}$)

$$\mathbf{H}_{r,q}(\xi, \rho) = \mathbf{C}\mathbf{\Phi}^{-1}(\xi, \rho)\mathbf{B} \text{ where } \mathbf{\Phi}(\xi, \rho) = \begin{bmatrix} \mathbf{J}_{\lambda,r}(\xi) & \mathbf{0} & \mathbf{0} \\ \mathbb{A} & \mathbf{J}_{\pi,q}^T(\rho) & \mathbf{0} \\ \mathbb{B} & \mathbf{0} & [\mathbf{J}_{\pi,q}(\rho), \boldsymbol{\tau}] \end{bmatrix}, \tag{26}$$

with $\mathbf{B} = [\mathbf{0}, \boldsymbol{\tau}, \mathbf{0}]^T \in \mathbb{R}^{N_{r,q}}$ and $\mathbf{C} = [0, \ldots, 0, -1] \in \mathbb{R}^{N_{r,q}}$. Moreover, the following holds (for $k = 1, \ldots, r$, $l = 1, \ldots, q$ and $\mathbf{w} = \mathrm{vect}(\Phi_{(11)})$)

$$\mathbb{A}_{:,k} = \begin{bmatrix} \mathbf{c}_{k,1} \\ \vdots \\ \mathbf{c}_{k,q+1} \end{bmatrix}, \mathbb{B}_{:,k} = \begin{bmatrix} \mathbf{c}_{k,1}\mathbf{w}_{k,1} \\ \vdots \\ \mathbf{c}_{k,q+1}\mathbf{w}_{k,q+1} \end{bmatrix} \text{ and } \boldsymbol{\tau}_k = \left(\prod_{l=1, l \neq k}^{q+1} \pi_k - \pi_l \right)^{-1} \tag{27}$$

and with

$$\mathbf{J}_{\eta,t}(x) = \begin{bmatrix} x-\eta_1 & \eta_2 - x & & \\ \vdots & & \ddots & \\ x-\eta_1 & & & \eta_{t+1}-x \end{bmatrix} \in \mathbb{C}^{t\times(t+1)}. \tag{28}$$

Notice that (26) only depends on the extended Loewner matrix null-space $\mathbf{c}$, the considered support points $\{\lambda_i\}_{i=1}^{r+1}$ and $\{\pi_j\}_{j=1}^{q+1}$ and the response data matrix $\{\Phi_{(11)}\}_{i,j=1}^{r+1,q+1}$. To stick with traditional tools deployed in simulation and control theory, one may also recover a descriptor realization $\mathcal{S}_{r,q}$ where all the parametric dependency is contained in the $\mathbf{A}_{r,q}(\rho)$ operator as [9]

$$\mathcal{S}_{r,q}: \begin{cases} \mathbf{E}_{r,q}\dot{\mathbf{x}}(t) = \mathbf{A}_{r,q}(\rho)\mathbf{x}(t) + \mathbf{B}_{r,q}\mathbf{u}(t)\ ,\ \mathbf{y}(t) = \mathbf{C}_{r,q}\mathbf{x}(t) \text{ where }, \\ \mathbf{E}_{r,q}, \mathbf{A}_{r,q}(\rho) \in \mathbb{C}^{N_{r,q}\times N_{r,q}}, \mathbf{B}_{r,q} \in \mathbb{C}^{N_{r,q}\times m}, \mathbf{C}_{r,q} \in \mathbb{C}^{p\times N_{r,q}}. \end{cases} \tag{29}$$

Remark 1 (Minimal realization in the multi-parametric case) *By inspecting (26), the realization is no longer identical to the one in the single variable case. Indeed in (26), the resolvant $\mathbf{\Phi}(\xi,\rho)$ includes both the dynamic and parametric variables, leading to a realization of order $N_{r,q}$ instead of r. Finding a minimal order realization is actually an unsolved problem so far. It has been investigated and is an important research field that can also be connected to the linear fractional transformation research one, largely used in the control community (see e.g. realization and control works [37, 47]).*

Remark 2 (SIMO and MISO cases) *The **SIMO** and **MISO** cases can also be addressed following the very same framework, by tangentially interpolating the data instead of the element-wisely (see §A.1 of [32] for details).*

Remark 3 (About the MIMO case) *The parametric extension to the **MIMO** case is not solved yet. Indeed, the tangential approach used in the non-parametric case and in most of multi-port interpolation frameworks [23, 54] is not applicable as is. Indeed, the realization construction is no longer applicable. An alternative approach is presented in [36] but which "only" interpolates a part of the data, namely $\Phi_{(11)}$, forgetting $\Phi_{(12)}$ and $\Phi_{(21)}$. This latter work also considers the same number of inputs and outputs.*

Example 3 (Reynolds parameter dependent linearized Navier-Stokes model) *Let us consider a fluid-flow configuration. It consists of a two-dimensional open square cavity flow problem where air flows from left to right for three different Reynolds numbers. Such a configuration, illustrated on Figure 1 (top right), is described in detail in the original work of [13] and in [49]. For simulation, Navier-Stokes equations are used along a mesh composed of $193,874$ triangles, corresponding to $n = 680,974$ degrees of freedom for the velocity variables along the x and y axis. After linearization around three fixed points for varying Reynolds numbers $Re = \{4000, 5250, 6000\}$ and discretization along the flow axis, three dynamical models $\{\mathbf{H}_l\}_{l=1}^{3}$ can be described as a **DAE** realization of order $n = 680,974$ where the input $\mathbf{u}(t)$ is the vertical pressure actuator located upstream of the cavity and the output $\mathbf{y}(t)$ is a shear stress sensor, located downstream of the cavity. Such a continuous-time n-th order realization for $l = \{1,2,3\}$ $\mathcal{S}_l : (\mathbf{E}, \mathbf{A}_l, \mathbf{B}, \mathbf{C}, \mathbf{0})$ where the parameter is the Reynolds number Re. In [49], the **IRKA** approach [30] (being a realization based $\mathcal{H}_2$-oriented reduction method) is used to sequentially approximate each realization with a low dimensional one. Then, the interpolation along the parameter is done in a second step by interpolating each coefficients in the canonical basis of the obtained realization.*

Here instead, the parametric Loewner framework is applied. The frequency response of each configuration along $\{z_k\}_{k=1}^{N} = z_0 \bigcup \{\imath\omega_k, -\imath\omega_k\}_{k=1}^{100}$, where $z_0 \in \mathbb{R}_+$ and ω_k logarithmically-spaced frequencies. Then, twenty intermediate configurations between each Reynolds numbers $Re = \{4000, 5250, 6000\}$ are constructed by linear interpolation. We obtain $\{z_k\}_{k=1}^{N=201}$, $\{p_l\}_{l=1}^{N=41}$ and thus $\Phi \in \mathbb{C}^{201\times 41}$. Our objective is to come up with a parametrized linear model that is able to faithfully reproduce the original transfer function data on a particular range of frequencies as well as on a target parameter range[5].

[5] Additional details and the data are available at https://morwiki.mpi-magdeburg.mpg.de/morwiki/index.php/Fluid_Flow_Linearized_Open_Cavity_Model

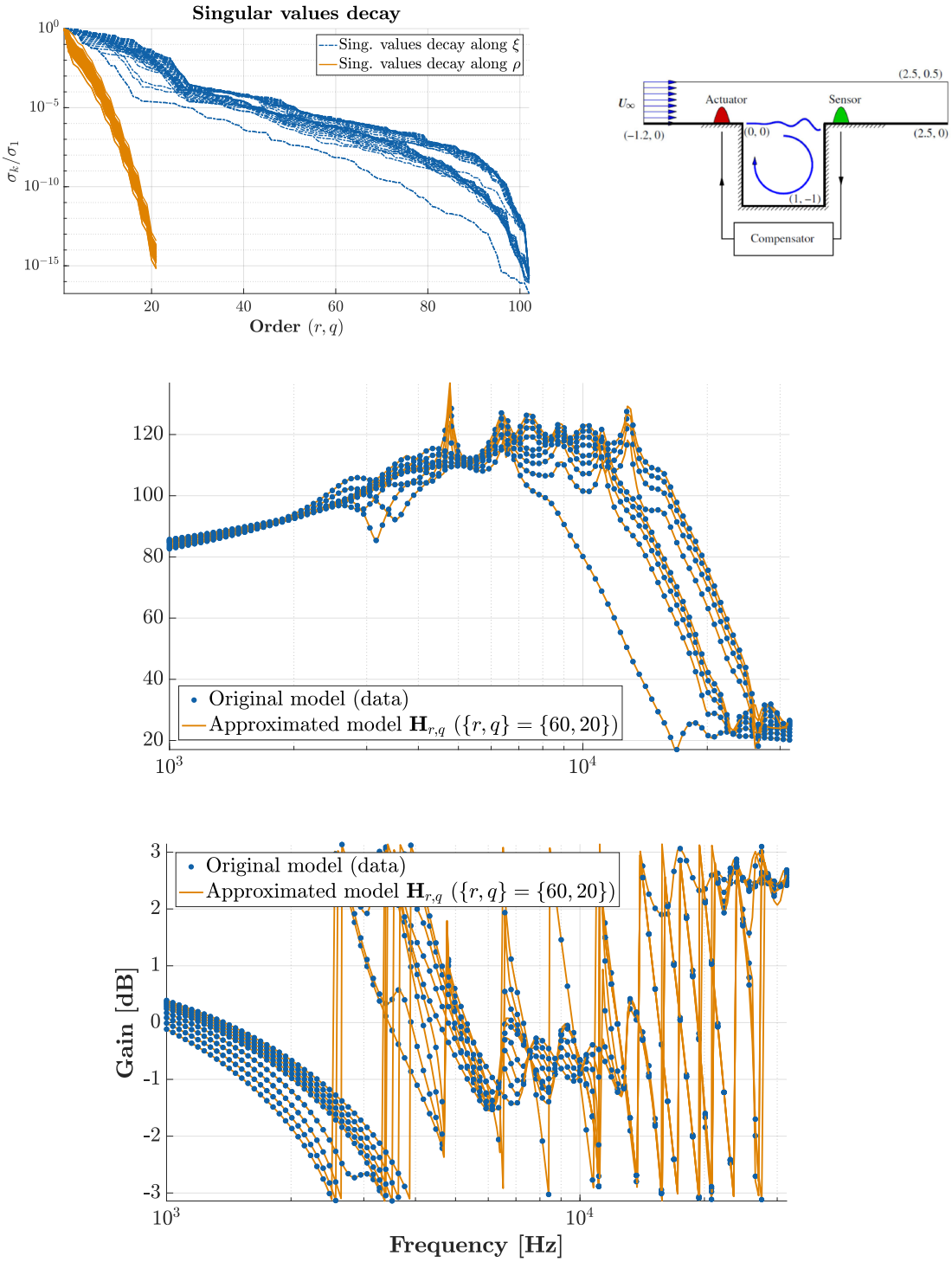

Figure 1: Top right: singular values drop of the one variable Loewner matrices (23). Top right: schematic view of the geometry (with illustration of the control structure used in [47]). Middle and bottom frames: frequency response gain and phase of the original sampled data (blue dots) and resulting parametric model $\mathbf{H}_{60,20}$ for some parametric values (solid orange lines).

On one hand, we form Loewner matrices by using measurements for varying frequency and constant parameter, while on the other hand we use varying parameter and constant frequency. Figure 1 (top left) depicts the two types of singular values. By investigating the drop in the singular values plot, we decide to use reduction orders $r = 30$ *and* $q = 20$ *for building the two dimensional Loewner matrix. As we want to find a real valued rational function rather than complex, the twice more support points are considered and realization size is increased. The reduced linear parametric model which is sampled over the same frequency and parameter range as before. When comparing to the original samples on Figure 1 (middle-bottom), the overall result is satisfactory, with a model of complexity* $r = 60$ *(instead of* $n = 680,974$*) an* $q = 20$ *(instead of a collection), enforcing a drastic memory saving, and hence, being a game changer for simulation and control design.*

2.4 Generalization to discrete-time models from time-domain data

For an LTI **SISO** system, let the impulse response be denoted with: $\mathbf{h} = \{ \cdots h_{-2}, h_{-1}, h_0, h_1, h_2, \cdots \}$. The associated system action $\mathcal{S}$ is given by the *convolution sum*:

$$\mathcal{S}: \ \mathbf{u} \longmapsto \mathbf{y} = \mathcal{S}(\mathbf{u}) = \mathbf{h} * \mathbf{u}, \ \text{ where } \ (\mathbf{h} * \mathbf{u})(t) = \sum_{k=-\infty}^{\infty} h_{t-k}\mathbf{u}(k), \ \ t \in \mathbb{Z}. \tag{30}$$

Here we restrict our attention to causal systems: $\mathbf{h}_k = 0$, $k < 0$; furthermore it is assumed that $\mathbf{u}(t) = 0$, $t < 0$. Hence, one can write that

$$\mathbf{y}(t) = h_0\mathbf{u}(t) + h_1\mathbf{u}(t-1) + \ \cdots \ + h_k\mathbf{u}(t-k) + \ \cdots \ , \ \ t \in \mathbb{Z}_+. \tag{31}$$

In the formulation above, h_j denotes the j^{th} Markov parameter of the underlying system. In the time domain, the data are samples of input and output signals

$$\mathbf{u}_N = [u_0, \ \cdots \ , \ u_{N-1}], \ \ \mathbf{y}_N = [y_0, \ \cdots \ , \ y_{N-1}], \tag{32}$$

where, for simplicity, we have used the shortened expressions $u_k := u(k)$ and $y_k := y(k)$. The system identification problem consists in recovering a discrete-time linear time invariant system compatible with the data in (32). We seek a minimal realization $(\mathbf{E}, \mathbf{A}, \mathbf{B}, \mathbf{C}, \mathbf{D})$:

$$\mathcal{S}_D : \mathbf{E}\,\mathbf{x}(t+1) = \mathbf{A}\mathbf{x}(t) + \mathbf{B}u(t), \ \ y(t) = \mathbf{C}\mathbf{x}(t) + \mathbf{D}u(t), \tag{33}$$

where $\mathbf{E}, \mathbf{A} \in \mathbb{R}^{n\times n}$, $\mathbf{B}, \mathbf{C}^T \in \mathbb{R}^{n\times 1}$, $\mathbf{D} \in \mathbb{R}$, and $\mathbf{x}(t) \in \mathbb{R}^n$ is the state; with the transfer function

$$\mathbf{H}(z) = \mathbf{C}(z\mathbf{E} - \mathbf{A})^{-1}\mathbf{B} + \mathbf{D} = \frac{b_m z^m + \cdots + b_1 z + b_0}{z^n + \cdots + a_1 z + a_0}, \ m \leq n. \tag{34}$$

The Markov parameters in (31) can be explicitly written in terms of matrices from the realization in (33), as follows:

$$h_0 = \mathbf{D}, \ \ h_k = \mathbf{C}\mathbf{A}^{k-1}\mathbf{B}, \ \forall k \geq 1. \tag{35}$$

Moreover, another interpretation of Markov parameters is that they encode the behavior of the transfer function in $\mathbf{H}(z)$ in (34) at $z = \infty$. More precisely, the values h_k's represent the coefficients of the following Laurent series expansion of the transfer function $\mathbf{H}(z)$:

$$\mathbf{H}(z) = h_0 + h_1 z^{-1} + h_2 z^{-2} + \cdots + h_k z^{-k} + \cdots \tag{36}$$

The first step in formulating the data-driven identification problem is to assemble the available input-output data into matrices with special format, i.e., Hankel matrices. Consequently, we introduce $\mathbf{U}_k \in \mathbb{R}^{M\times L}$, $\mathbf{Y}_k \in \mathbb{R}^{M\times L}$ for any $k \geq 0$, as follows

$$\mathbf{U}_k = \begin{bmatrix} u_k & u_{k+1} & \cdots & u_{k+L-1} \\ u_{k+1} & u_{k+2} & \cdots & u_{k+L} \\ \vdots & \vdots & \ddots & \vdots \\ u_{k+M-1} & u_{k+M} & \cdots & u_{k+M+L-2} \end{bmatrix}, \mathbf{Y}_k = \begin{bmatrix} y_k & y_{k+1} & \cdots & y_{k+L-1} \\ y_{k+1} & y_{k+2} & \cdots & y_{k+L} \\ \vdots & \vdots & \ddots & \vdots \\ y_{k+M-1} & y_{k+M} & \cdots & y_{k+M+L-2} \end{bmatrix}. \tag{37}$$

Theorem 1 *The following results are given in [31]. If $M \geq n + rank\,\mathbf{U}_0$, and $z \in \mathbb{C}$, then the following holds true:*

(a) $rank\,[z\mathbf{Y}_0 - \mathbf{Y}_1, \mathbf{U}_0] = n + rank\,\mathbf{U}_0$, and the rank decreases by one if z is a pole.

(b) Let $\mathbf{\Pi}_{\mathbf{U}_0}$ be the orthogonal projection onto the column space of $\mathbf{U}_0$. Then the system poles p_j are the n finite generalized eigenvalues of the singular pencil

$$z\mathbf{Q}_0 - \mathbf{Q}_1 = (\mathbf{I} - \mathbf{\Pi}_{\mathbf{U}_0})(z\mathbf{Y}_0 - \mathbf{Y}_1), \tag{38}$$

where $rank\,\mathbf{Q}_0 = rank\,\mathbf{Q}_1 = n$. It also follows that matrices $\mathbf{Q}_0$, $\mathbf{Q}_1$ have the same column and row spaces.

In order to be able to accurately extract system invariants (poles, residues, Markov parameters, etc.) from input-output data, there are certain conditions that need to be imposed to sequence of control inputs applied. For example, one of such conditions is the so-called *persistence of excitation*. However, as explained in [31], this requirement of the input is not necessary when the initial conditions are zero, i.e. the system is at rest before the input is applied: $\mathbf{u}(t) = 0$ and $\mathbf{y}(t) = 0$, for $t < 0$. This assumption is equivalent to $\mathbf{x}(0) = 0$.

Next, as explained in [31], there exists matrix $\mathbf{Y}$, such that the matrix pencil $(\widehat{\mathbf{Q}}_0, \widehat{\mathbf{Q}}_1)$, where $\widehat{\mathbf{Q}}_0 = \mathbf{Y}^*\mathbf{Q}_0$, $\widehat{\mathbf{Q}}_1 = \mathbf{Y}^*\mathbf{Q}_1$, is *r*egular (often $\widehat{\mathbf{Q}}_0$, $\widehat{\mathbf{Q}}_1$ can be taken as the leading $n \times n$ sub-matrices of $\mathbf{Q}_0$, $\mathbf{Q}_1$). The following result in [31] gives a realization for a model of dimension n:

Theorem 2 *For zero initial conditions, the system has a minimal realization*

$$\widetilde{\mathbf{E}} = \widehat{\mathbf{Q}}_0, \quad \widetilde{\mathbf{A}} = \widehat{\mathbf{Q}}_1, \quad \widetilde{\mathbf{B}} = \mathbf{q}_0, \quad \widetilde{\mathbf{C}} = [h_1, \cdots, h_n], \quad \widetilde{\mathbf{D}} = h_0,$$

where $\mathbf{q}_0$ is the first column of $\widehat{\mathbf{Q}}_0$ and the Markov parameters h_j's are obtained by solving the following linear system of equations

$$\begin{bmatrix} u_0 & & & \\ u_1 & u_0 & & \\ \vdots & \ddots & \ddots & \\ u_n & \cdots & u_1 & u_0 \end{bmatrix} \begin{bmatrix} h_0 \\ h_1 \\ \vdots \\ h_n \end{bmatrix} = \begin{bmatrix} y_0 \\ y_1 \\ \vdots \\ y_n \end{bmatrix}. \tag{39}$$

In this case, the solution of a lower triangular system of equations is needed. It readily follows that the Markov parameters can be computed for any input $\mathbf{u}$. For more details on this procedure, we refer the reader to [31].

The result stated in Theorem 2 can indeed be further specialized for the case when of a very special input given by $\mathbf{u} = [1, 0, \cdots, 0]$. Hence, when the input is an impulse, the output is a finite sequence of Markov parameters, i.e., $\mathbf{y} = [h_0, h_1, \cdots, h_{N-1}]$. The realization in Theorem 2 is hence modified appropriately, since the matrix pencil is given by two Hankel matrices. Now, let $\tilde{\mathcal{S}}_n$ be the new realization given by

$$\widetilde{\mathbf{E}} = \begin{bmatrix} h_1 & h_2 & \cdots & h_n \\ h_2 & h_3 & \cdots & h_{n+1} \\ \vdots & \vdots & \ddots & \vdots \\ h_n & h_{n+1} & \cdots & h_{2n-1} \end{bmatrix}, \widetilde{\mathbf{A}} = \begin{bmatrix} h_2 & h_3 & \cdots & h_{n+1} \\ h_3 & h_4 & \cdots & h_{n+2} \\ \vdots & \vdots & \ddots & \vdots \\ h_{n+1} & h_{n+2} & \cdots & h_{2n} \end{bmatrix},$$
$$\widetilde{\mathbf{C}} = \begin{bmatrix} h_1, & h_2, \cdots, & h_n \end{bmatrix}, \quad \widetilde{\mathbf{B}} = \widetilde{\mathbf{C}}^T, \quad \widetilde{\mathbf{D}} = h_0. \tag{40}$$

As in Section 2.2, we could further reduce the dimension of the fitted model in (40) by means of projection (compressing the realization of order n to one of order r by means of orthogonal matrices computed using the **SVD**). In this case, we talk about approximation, i.e. fitting a model which approximately explains the data. Hence, let $\mathbf{Y} \in \mathbb{R}^{n\times r}$ (resp. $\mathbf{X} \in \mathbb{R}^{n\times r}$) be the matrix containing the first r left and respectively, right singular vectors of the Hankel matrix denoted in (40) by $\widetilde{\mathbf{E}}$. The reduced-order realization $\tilde{\mathcal{S}}_r : (\tilde{\mathbf{E}}_r, \tilde{\mathbf{A}}_r, \tilde{\mathbf{B}}_r, \tilde{\mathbf{C}}_r, \mathbf{0})$ is computed as follows

$$\tilde{\mathbf{E}}_r = \mathbf{Y}^T\tilde{\mathbf{E}}\mathbf{X}\,, \tilde{\mathbf{A}}_r = \mathbf{Y}^T\tilde{\mathbf{A}}\mathbf{X}\,, \tilde{\mathbf{B}}_r = \mathbf{Y}^T\tilde{\mathbf{B}}\,, \tilde{\mathbf{C}}_r = \tilde{\mathbf{C}}\mathbf{X}, \text{ and } \tilde{\mathbf{D}}_r = h_0. \tag{41}$$

Example 4 (A structural mechanics model) *As a numerical test case, we consider the model of a building (the Los Angeles University Hospital) from the SLICOT MOR benchmark collection. The building has 8 floors, each having 3 degrees of freedom, i.e, displacements in x and y directions, and rotation. The original model is hence a second-order linear system of dimension* $n_0 = 24$. *It can be written equivalently as a first-order linear system of dimension* $n = 48$. *We slightly modify the original model by scaling the vector* $\mathbf{B} \in \mathbb{R}^{48}$ *with* 10^4.

The numerical treatment goes as follows: the original continuous-time LTI model of dimension $n = 48$ *is discretized using a classical Backward Euler first order scheme. The simulation time horizon is* $[0, 5]$*s, while the time step is* $\Delta t = 4 \cdot 10^{-3}$. *The control input is chosen to be* $u(t) = \frac{1}{10}\big(\cos(50t) + 2\cos(20t) + 3\cos(10t)\big)$. *Hence, by means of this time-domain simulation, we collect* $N = 2001$ *measurements of the discretized input and output, i.e.,as in 32. These values are depicted in the upper pane of Fig. 2. The Markov parameters are extracted by following the approach in (39), and are depicted in the lower pane of Fig. 2 (there, the magnitude of the error between the true Markov parameters and the estimated ones is shown in orange).*

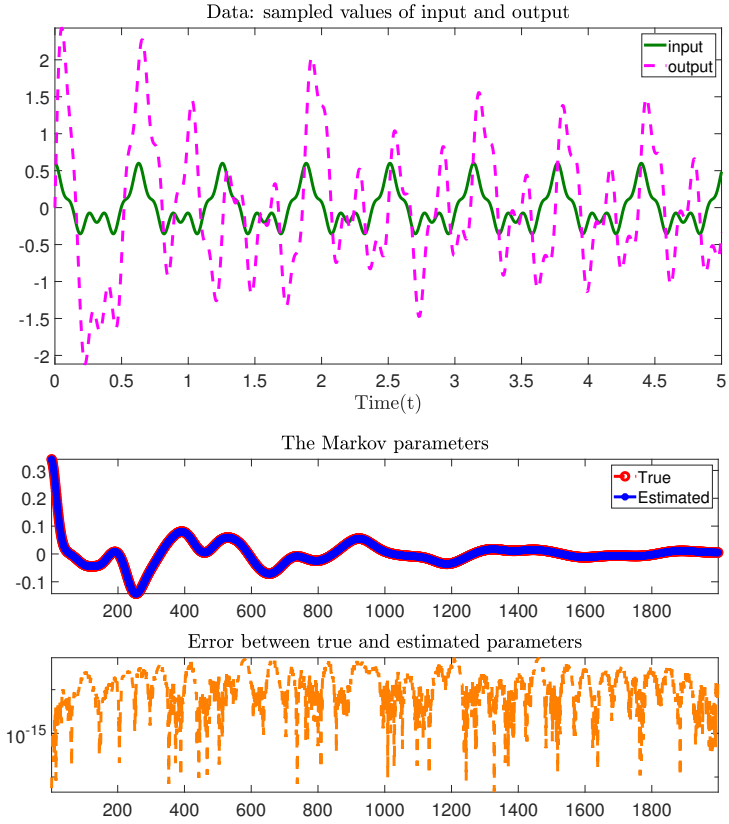

Figure 2: Samples of the input and output signals (up) and the true and recovered Markov parameters (down).

Next, form a 1000×1000 *Hankel matrix as in (40). The decay of its singular values is displayed in the upper pane of Fig. 3. Then, choose the truncation order* $r = 20$, *and construct a realization of order r as presented in (41). Finally, convert this discrete-time model back to the continuous time, and compare the frequency response of the original model of order n, with that of the reduced one of order r (on a range of 500 frequency points in the interval* $[10^0, 10^2]$*). The results (frequency responses and the approximation error) are presented in the lower pane of Fig. 3. Indeed, the model is well approximated by means of the proposed method.*

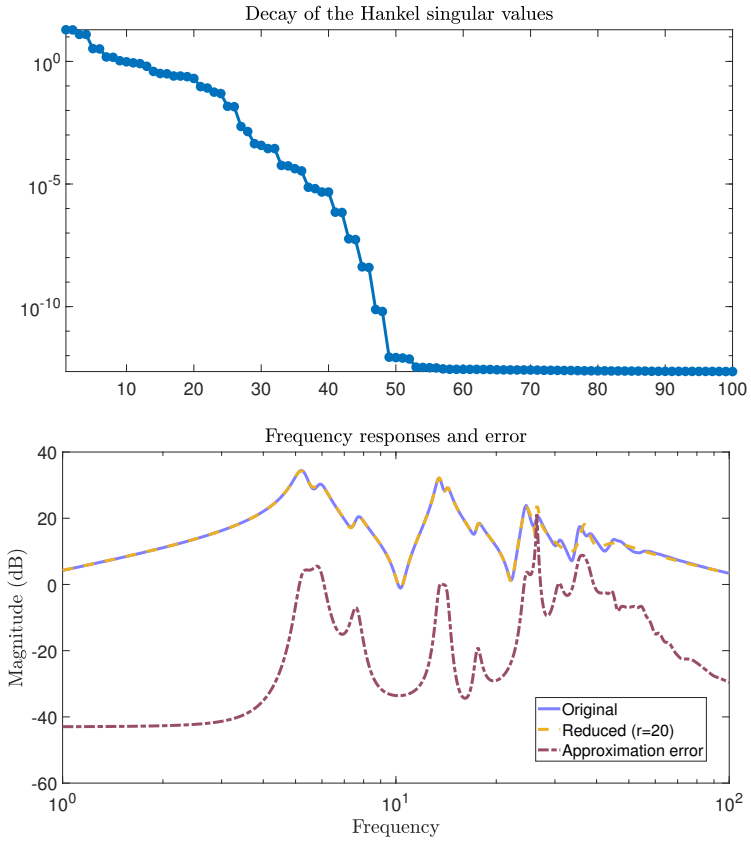

Figure 3: Decay of the Hankel singular values (up) and frequency responses computations: original, reduced and the approximation error (down).

2.5 Extensions to nonlinear systems

Consider a nonlinear system described by the following equations

$$\mathcal{S}_N : \begin{cases} \dot{\mathbf{x}}(t) = \mathbf{f}(\mathbf{x}(t)) + \mathbf{g}(\mathbf{x}(t))\mathbf{u}(t), \\ \mathbf{y}(t) = \mathbf{C}\mathbf{x}(t), \end{cases} \tag{42}$$

where $t \geqslant 0$, $\mathbf{x}(0) = \mathbf{x}_0$ and the nonlinear functions $\mathbf{f}, \mathbf{g} : \mathbb{R}^n \rightarrow \mathbb{R}^n$ are assumed to be analytic in $\mathbf{x}(t)$. We also assume that the output depends linearly on the variable $\mathbf{x}(t)$, i.e., $\mathbf{y}(t) = \mathbf{C}\mathbf{x}(t)$.

In this section, we will focus on a recent extension of the Loewner framework to reducing bilinear systems. The motivation for this choice is that any smooth, nonlinear system with analytical nonlinearities can be approximated by a bilinear system. This is accomplished by means of a technique, commonly known as Carleman linearization (see [18, 52]). Since this is based on Taylor expansion and truncation, the resulting bilinear system will approximate the original nonlinear system depending on the number of terms kept in the expansion. In many practical applications, approximating the original system is sufficient for a large variety of tasks. We proceed by writing the truncated *Taylor series* for the non-linear functions $\mathbf{f}$ and $\mathbf{g}$, where N represents the truncation index, i.e.

$$\begin{cases} \mathbf{f}(\mathbf{x}) = \sum_{k=1}^{N} \mathbf{F}_k \mathbf{x}^{(N)} = \mathbf{F}_1\mathbf{x} + \mathbf{F}_2\mathbf{x}^{(2)} + \ldots + \mathbf{F}_N\mathbf{x}^{(N)}, \\ \mathbf{g}(\mathbf{x}) = \sum_{k=0}^{N-1} \mathbf{G}_k \mathbf{x}^{(k)} = \mathbf{G}_0 + \mathbf{G}_1\mathbf{x} + \ldots + \mathbf{G}_{N-1}\mathbf{x}^{(N-1)}. \end{cases} \tag{43}$$

where $\mathbf{G}_0 \in \mathbb{R}^{n\times 1}, \mathbf{F}_j, \mathbf{G}_j \in \mathbb{R}^{n^j \times n^j}$, $j \geqslant 1$. Here, $\mathbf{F}_1, \mathbf{G}_1$ denote the Jacobian matrices of $\mathbf{f}$ and $\mathbf{g}$, respectively, and $\mathbf{F}_k, \mathbf{G}_k$ denote the matrices of higher derivatives. Moreover $\mathbf{x}^{(k)}$ denotes the Kronecker product of the state variable $\mathbf{x}$ with itself (k times). The next step is to introduce a new state variable $\mathbf{x}^{\otimes}(t)$ as

$$\mathbf{x}^{\otimes}(t) = \begin{bmatrix} \mathbf{x}(t) & \mathbf{x}^{(2)}(t) & \ldots & \mathbf{x}^{(N)}(t) \end{bmatrix}^T \in \mathbb{R}^{n^{(N)}},$$

where $n^{(N)} = n + n^2 + ... + n^N = \frac{n^N - n}{n-1}$. This is obtained by concatenating all higher powers of vector $\mathbf{x}$ (up to N). In this way, by computing derivatives of $\mathbf{x}^{(k)}$, we obtain a bilinear system with the following realization

$$\begin{cases} \dot{\mathbf{x}}^{\otimes}(t) &= \mathbf{A}^{\otimes}\mathbf{x}^{\otimes}(t) + \mathbf{N}^{\otimes}\mathbf{x}^{\otimes}(t)\mathbf{u}(t) + \mathbf{B}^{\otimes}\mathbf{u}(t), \\ \mathbf{y} &= \mathbf{C}^{\otimes}\mathbf{x}^{\otimes}(t), \end{cases} \tag{44}$$

where $\mathbf{x}^{\otimes}(0) = \mathbf{0}$ and the matrices $\mathbf{A}^{\otimes}, \mathbf{N}^{\otimes} \in \mathbb{R}^{n^{(N)} \times n^{(N)}}$, $\mathbf{B}^{\otimes}$, $\left(\mathbf{C}^{\otimes}\right)^T \in \mathbb{R}^{n^{(N)}}$ are as in Section 2.1.1 of [27]. In what follows, we employ a more generic definition of *b*ilinear systems $\mathcal{S}_{\mathrm{B}} = (\mathbf{C}, \mathbf{E}, \mathbf{A}, \mathbf{N}, \mathbf{B})$, characterized by:

$$\mathcal{S}_B: \quad \mathbf{E}\dot{\mathbf{x}}(t) = \mathbf{A}\mathbf{x}(t) + \mathbf{N}\mathbf{x}(t)\mathbf{u}(t) + \mathbf{B}\mathbf{u}(t), \quad \mathbf{y}(t) = \mathbf{C}\mathbf{x}(t), \tag{45}$$

where $\mathbf{E},\ \mathbf{A},\ \mathbf{N} \in \mathbb{R}^{n\times n}$, $\mathbf{B} \in \mathbb{R}^{n\times m}$, $\mathbf{C} \in \mathbb{R}^{p\times n}$ and $\mathbf{x} \in \mathbb{R}^n$, $\mathbf{u},\ \mathbf{y} \in \mathbb{R}$. The matrix $\mathbf{E}$ is assumed to be non-singular. Also, for simplicity of exposition, we will discuss only the **SISO** case. More details on bilinear system model order reduction can be found in [14, 17, 21]. Bilinear systems as in (45) are equivalent an infinite collection of coupled linear time-varying systems of the form:

$$\mathbf{E}\dot{\mathbf{x}}_1(t) = \mathbf{A}\mathbf{x}_1(t) + \mathbf{B}\mathbf{u}(t), \quad \mathbf{E}\dot{\mathbf{x}}_i(t) = \mathbf{A}\mathbf{x}_i(t) + \mathbf{N}\mathbf{x}_{i-1}(t)\mathbf{u}(t),\ i \geq 2. \tag{46}$$

The time-varying factor appears only in the matrices that scale the control input $\mathbf{u}(t)$ at each level $i \geq 2$. Based on (46), the solution of (45) is decomposed as $\mathbf{x}(t) = \sum_{i=1}^{\infty} \mathbf{x}_i(t)$. Furthermore, the input-output representation of the bilinear system $\mathcal{S}_{\mathrm{B}}$ can be expressed in terms of the *Volterra series representation* ([21, 52]). Moreover, considering $\mathbf{x}_{\ell-1}(t)$ in the ℓ^{th} equation as a pseudo-input for $l = 1, 2, \ldots$, the frequency-domain behavior is described by a series of generalized transfer functions as given also in [6, 21, 52]:

$$\mathbf{H}_\ell(s_1, s_2, \ldots, s_\ell) = \mathbf{C}\,\mathbf{\Phi}(s_1)\,\mathbf{N}\,\mathbf{\Phi}(s_2)\,\mathbf{N}\ \cdots\ \mathbf{N}\,\mathbf{\Phi}(s_\ell)\,\mathbf{B}, \tag{47}$$

where the *r*esolvent of the pencil $(\mathbf{A}, \mathbf{E})$ is denoted by $\mathbf{\Phi}(\xi) = (\xi\mathbf{E} - \mathbf{A})^{-1}$. The characterization of bilinear systems by means of the rational functions in (47) suggests that reduction of such systems can be performed by means of the Loewner framework. In what follows, we will review some highlights of the procedure originally presented in [6]. We use the concept of multi-tuples, composed of multiple interpolation points corresponding to evaluations of the transfer functions in (47). For simplicity, we will assume that one set of right multi-tuples $\boldsymbol{\lambda}$, and one set of left multi-tuples $\boldsymbol{\mu}$ with the same number of interpolation points (denoted with k), are given as

$$\begin{aligned} \boldsymbol{\lambda} &= \{\{\lambda_1\}, \{\lambda_2, \lambda_1\},\ \ldots,\ \{\lambda_k, \ldots, \lambda_2, \lambda_1\}\}, \\ \boldsymbol{\mu} &= \{\{\mu_1\}, \{\mu_1, \mu_2\},\ \ldots,\ \{\mu_1, \mu_2, \ldots, \mu_k\}\}. \end{aligned} \tag{48}$$

For the tuples in (48), we introduce the associated generalized controllability and observability matrices, denoted with $\mathcal{R} \in \mathbb{C}^{n\times k}$, and respectively with $\mathcal{O} \in \mathbb{C}^{k\times n}$, as in [6], i.e.:

$$\begin{aligned} \mathcal{R} &= [\ \mathbf{\Phi}(\lambda_1)\mathbf{B},\ \mathbf{\Phi}(\lambda_2)\mathbf{N}\mathbf{\Phi}(\lambda_1)\mathbf{B},\ \cdots,\ \mathbf{\Phi}(\lambda_k)\mathbf{N}\mathbf{\Phi}(\lambda_{k-1})\mathbf{N}\cdots\mathbf{N}\mathbf{\Phi}(\lambda_1)\mathbf{B}], \\ \mathcal{O} &= \begin{bmatrix} \mathbf{C}\mathbf{\Phi}(\mu_1) \\ \mathbf{C}\mathbf{\Phi}(\mu_1)\mathbf{N}\mathbf{\Phi}(\mu_2) \\ \vdots \\ \mathbf{C}\mathbf{\Phi}(\mu_1)\mathbf{N}\mathbf{\Phi}(\mu_2)\mathbf{N}\ \cdots\ \mathbf{N}\mathbf{\Phi}(\mu_k) \end{bmatrix}. \end{aligned} \tag{49}$$

As shown in [6], the matrices $\mathcal{R}$ and $\mathcal{O}$ defined in (49), satisfy the following generalized Sylvester equations:

$$\begin{aligned} \mathbf{A}\,\mathcal{R} + \mathbf{N}\,\mathcal{R}\,\mathbf{S}_{\mathbf{R}} + \mathbf{B}\,\mathbf{R} &= \mathbf{E}\,\mathcal{R}\,\mathbf{\Lambda} \\ \mathcal{O}\,\mathbf{A} + \mathbf{S}_{\mathbf{L}}\,\mathcal{O}\,\mathbf{N} + \mathbf{L}\,\mathbf{C} &= \mathbf{M}\,\mathcal{O}\,\mathbf{E}. \end{aligned} \tag{50}$$

2.5.1 The generalized Loewner pencil

Given the above notations, we introduce the following matrices, i.e., the generalized Loewner matrix $\mathbb{L}$, and the generalized shifted Loewner matrix $\mathbb{M}$

$$\mathbb{L} = -\mathcal{O}\,\mathbf{E}\,\mathcal{R} \in \mathbb{C}^{k\times k}, \quad \mathbb{M} = -\mathcal{O}\,\mathbf{A}\,\mathcal{R} \in \mathbb{C}^{k\times k}. \tag{51}$$

In addition we define the quantities

$$\mathbb{T} = O\,\mathbf{N}\,\mathcal{R} \in \mathbb{C}^{k\times k}, \quad \mathbb{V} = O\,\mathbf{B} \in \mathbb{C}^{k} \quad \text{and} \quad \mathbb{W} = \mathbf{C}\,\mathcal{R} \in \mathbb{C}^{1\times k}. \tag{52}$$

Note that $\mathbb{L}$ and $\mathbb{M}$ as defined above are indeed Loewner matrices, that is, they can be expressed as divided differences of appropriate transfer function values of the underlying bilinear system; the following equalities hold:

$$\begin{aligned}\mathbb{L}(j,i) &= \frac{\mathbf{H}_{j+i-1}(\mu_1,\ldots,\mu_j,\lambda_{i-1},\ldots,\lambda_1) - \mathbf{H}_{j+i-1}(\mu_1,\ldots,\mu_{j-1},\lambda_i,\ldots,\lambda_1)}{\mu_j-\lambda_i}\\ \mathbb{M}(j,i) &= \frac{\mu_j\mathbf{H}_{j+i-1}(\mu_1,\ldots,\mu_j,\lambda_{i-1},\ldots,\lambda_1) - \lambda_i\mathbf{H}_{j+i-1}(\mu_1,\ldots,\mu_{j-1},\lambda_i,\ldots,\lambda_1)}{\mu_j-\lambda_i},\end{aligned} \tag{53}$$

while $\mathbf{V}(j,1) = \mathbf{H}_j(\mu_1,\ldots,\mu_{j-1},\mu_j)$, $\mathbf{W}(1,i) = \mathbf{H}_i(\lambda_i,\lambda_{i-1},\ldots,\lambda_1)$, and $\mathbb{T}(j,i) = \mathbf{H}_{j+i}(\mu_1,\ldots,\mu_{j-1},\mu_j,\lambda_i,\lambda_{i-1},\ldots,\lambda_1)$. This result shows that all quantities of the bilinear Loewner surrogate model can be indeed computed using only data, and the realization is written concisely as

$$\hat{\mathbf{E}} = -\mathbb{L}, \quad \hat{\mathbf{A}} = -\mathbb{M}, \quad \hat{\mathbf{N}} = \mathbb{T}, \quad \hat{\mathbf{B}} = \mathbb{V}, \quad \hat{\mathbf{C}} = \mathbb{W}. \tag{54}$$

It was shown in [6], that the bilinear model of dimension k in (54) matches a total of $2k + k^2$ transfer function values of the original bilinear system of dimension n.

If necessary, the model given is (54) is further reduced similarly to the classical linear case, e.g., as in (12). This is done by projecting with special matrices using the singular value decay of the Loewner pencil involved. This provides a useful indicator for choosing the truncation order ([6]).

Example 5 (An illustrative example) *Given a **SISO** bilinear system as in (45), given by* $(\mathbf{C},\mathbf{E},\mathbf{A},\mathbf{N},\mathbf{B})$ *of order n, consider the tuples of left and right interpolation points:* $\begin{bmatrix} \{\mu_1\} & \{\mu_1,\mu_2\} \end{bmatrix}$, $\begin{bmatrix} \{\lambda_1\}, & \{\lambda_2,\lambda_1\} \end{bmatrix}$. *The generalized observability and controllability matrices are*

$$\begin{aligned} O &= \begin{bmatrix} \mathbf{C}(\mu_1\mathbf{E}-\mathbf{A})^{-1} \\ \mathbf{C}(\mu_1\mathbf{E}-\mathbf{A})^{-1}\mathbf{N}(\mu_2\mathbf{E}-\mathbf{A})^{-1} \end{bmatrix},\\ \mathcal{R} &= \begin{bmatrix} (\lambda_1\mathbf{E}-\mathbf{A})^{-1}\mathbf{B}, & (\lambda_2\mathbf{E}-\mathbf{A})^{-1}\mathbf{N}(\lambda_1\mathbf{E}-\mathbf{A})^{-1}\mathbf{B} \end{bmatrix}. \end{aligned}$$

The Loewner model matrices can be written in terms of data as:

$$\mathbb{L} = \begin{bmatrix} \frac{\mathbf{H}_1(\mu_1)-\mathbf{H}_1(\lambda_1)}{\mu_1-\lambda_1} & \frac{\mathbf{H}_2(\mu_1,\lambda_1)-\mathbf{H}_2(\lambda_2,\lambda_1)}{\mu_1-\lambda_2} \\ \frac{\mathbf{H}_2(\mu_1,\mu_2)-\mathbf{H}_2(\mu_1,\lambda_1)}{\mu_2-\lambda_1} & \frac{\mathbf{H}_3(\mu_1,\mu_2,\lambda_1)-\mathbf{H}_3(\mu_1,\lambda_2,\lambda_1)}{\mu_2-\lambda_2} \end{bmatrix} = -O\mathbf{E}\mathcal{R},$$

$$\mathbb{M} = \begin{bmatrix} \frac{\mu_1\mathbf{H}_1(\mu_1)-\lambda_1\mathbf{H}_1(\lambda_1)}{\mu_1-\lambda_1} & \frac{\mu_1\mathbf{H}_2(\mu_1,\lambda_1)-\lambda_2\mathbf{H}_2(\lambda_2,\lambda_1)}{\mu_1-\lambda_2} \\ \frac{\mu_2\mathbf{H}_2(\mu_1,\mu_2)-\lambda_1\mathbf{H}_2(\mu_1,\lambda_1)}{\mu_2-\lambda_1} & \frac{\mu_2\mathbf{H}_3(\mu_1,\mu_2,\lambda_1)-\lambda_2\mathbf{H}_3(\mu_1,\lambda_2,\lambda_1)}{\mu_2-\lambda_2} \end{bmatrix} = -O\mathbf{A}\mathcal{R},$$

$$\mathbb{T} = \begin{bmatrix} \mathbf{H}_2(\mu_1,\mu_2) & \mathbf{H}_3(\mu_1,\lambda_2,\lambda_1) \\ \mathbf{H}_3(\mu_1,\mu_2,\lambda_1) & \mathbf{H}_4(\mu_1,\mu_2,\lambda_2,\lambda_1) \end{bmatrix} = O\mathbf{N}\mathcal{R},$$

$$\mathbb{V} = \begin{bmatrix} \mathbf{H}_1(\mu_1) \\ \mathbf{H}_2(\mu_1,\mu_2) \end{bmatrix} = O\mathbf{B}, \quad \mathbb{W} = \begin{bmatrix} \mathbf{H}_1(\lambda_1) & \mathbf{H}_2(\lambda_2,\lambda_1) \end{bmatrix} = \mathbf{C}\mathcal{R}.$$

The surrogate bilinear system constructed as in (54) matches eight transfer function values (47) of the original system, namely:

$$\begin{aligned} \textit{two of } \mathbf{H}_1: &\quad \mathbf{H}_1(\mu_1),\ \mathbf{H}_1(\lambda_1),\\ \textit{three of } \mathbf{H}_2: &\quad \mathbf{H}_2(\mu_1,\mu_2),\ \mathbf{H}_2(\mu_1,\lambda_1),\ \mathbf{H}_2(\lambda_2,\lambda_1),\\ \textit{two of } \mathbf{H}_3: &\quad \mathbf{H}_3(\mu_1,\mu_2,\lambda_1),\ \mathbf{H}_3(\mu_1,\lambda_2,\lambda_1),\ \textit{and}\\ \textit{one of } \mathbf{H}_4: &\quad \mathbf{H}_4(\mu_1,\mu_2,\lambda_2,\lambda_1). \end{aligned}$$

Example 6 (Viscous (bi)linearized Burgers' equation model) *We choose as a numerical test-case example, a discretized model of the viscous Burgers' equation (previously presented also in [6]). The original partial differential equation is given by*

$$\frac{\partial v(x,t)}{\partial t} + v(x,t)\frac{\partial v(x,t)}{\partial x} = \frac{\partial}{\partial x}\left(\nu \frac{v(x,t)}{\partial x}\right), \quad (x,t) \in (0,1)\times(0,T)\ , \tag{55}$$

subject to the initial and boundary conditions given by

$$v(x,0) = f(x),\ x \in [0,1],\ v(0,t) = u(t),\ v(1,t) = 0,\ t \geqslant 0\ .$$

The above system occurs in the area of fluid dynamics where it can be used for modeling gas dynamics and traffic flow. The solution $v(x,t)$ can be interpreted as a function describing the velocity at (x,t). In general, the viscosity coefficient $\nu(x,t)$ might depend on space and time as well.

Some simplifications are performed, and the viscosity coefficient $\nu(x,t) = \nu$ is assumed to be constant. Furthermore, a zero initial condition on the system, i.e., $f(x) = 0$, is considered. Finally, we assume that the left boundary is subject to a control.

Start with a spatial discretization of equation (55), using an equidistant step size $h = \frac{1}{n+1}$ where n denotes the number of interior points of the interval $(0,1)$. By using first-order derivative approximations schemes, a nonlinear model is obtained (with quadratic-bilinear nonlinearities). Next, use the Carleman bilinearization technique to approximate this n^{th}order nonlinear system with a bilinear system of order $N = n^2 + n$.

Denote with Σ_B the 4970^{th} order initial bilinear system obtained by means of the Carleman bilinearization. The first step is to collect samples from generalized bilinear transfer functions up to order two; the 400 interpolations points are chosen logarithmically spaced in the interval $[10^{-3}, 10^{3}]\imath$. Next, we construct the bilinear Loewner matrices as presented in this section, and display the singular value decay in the upper pane of Fig. 4. We construct a reduced-order model of order $r = 32$; the poles are depicted in the lower pane of Fig. 4.

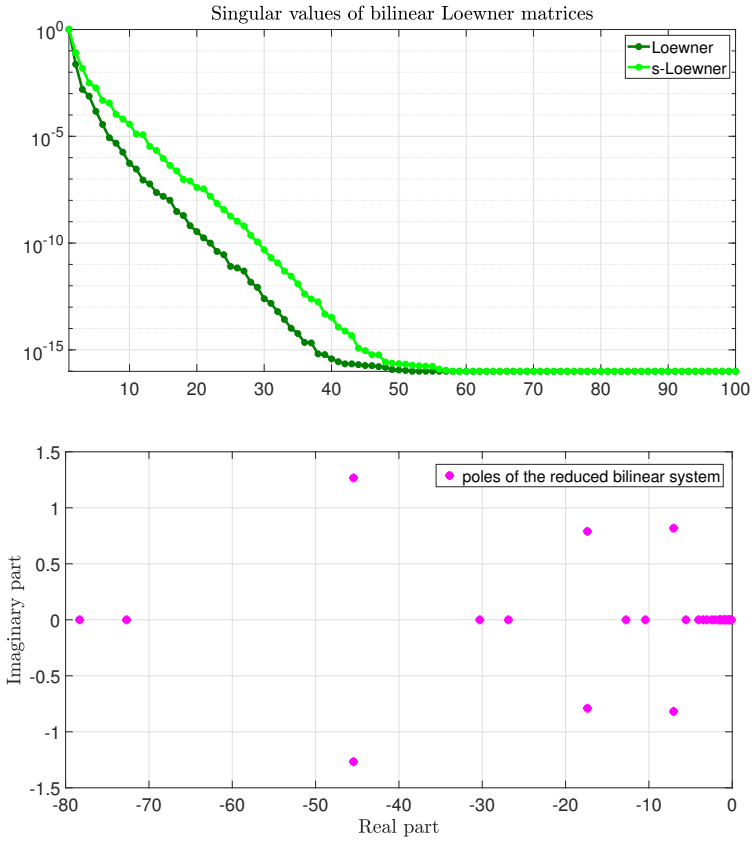

Figure 4: The first 100 singular values of the Loewner matrices (up) and the poles of the reduced-order model (down).

Finally, perform a time-domain simulation for a control input given by $u(t) = \frac{1}{5}(\cos(2\pi t) + \sin(20\pi t)e^{-t/5})$, and on a chosen time span of $[0,10]s$. The observed outputs for both the original and of the reduced-order

bilinear systems are displayed in the upper pane of Fig. 5, while the approximation error is depicted in the lower pane of Fig. 5.

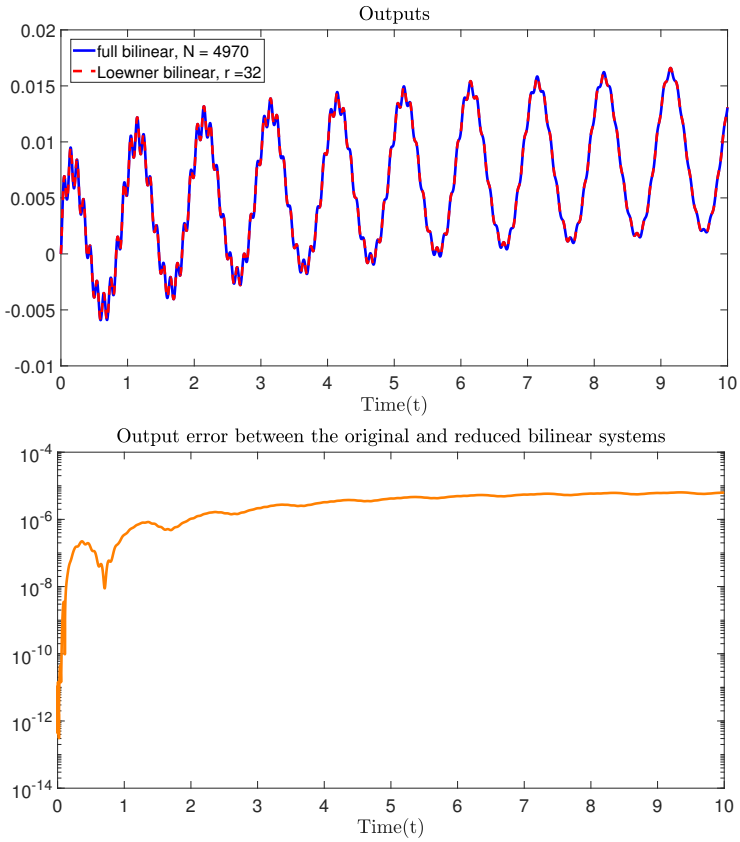

Figure 5: Time-domain simulations: the observed outputs (up) and the approximation error in the time domain (down).

3 Examples of model reduction of large-scale systems

In this section, we will demonstrate how Loewner-based rational approximation and reduction features have been successfully applied on real-life industrial problems. First, two benchmarks sequentially involving a generic business jet aircraft model and measurements data obtained by Dassault-Aviation, a French aircraft supplier, are considered (see [40, 41, 48, 50]). Second, a benchmark involving a simplified open channel model constructed by Electricité De France, the French electricity supplier is involved (see [19]). More specifically, a gust oriented model described by an non-rational transfer function is considered (section 3.1), then ground vibration experimental data (in section 3.2) and finally, linear partial differential equations (in section 3.3).

3.1 Gust load oriented generic business jet aircraft model

An important aircraft design criterion concerns the so-called *gust load envelope* monitoring. Prior to any test or exploitation, aircraft structural integrity should be guaranteed. One important certificate is to preserve and limit the worst case loads along the wings in response to vertical gust episodes. To this aim, it is standard to consider vertical gust disturbances $\mathbf{w}$, modelled through the so-called "1-cosine" profiles [50]. The *gust load envelope* is simply the worst case load responses along the wing span in reaction to the set of many differently chosen time-domain vertical wind gust profiles affecting the aircraft structure. In the preliminary conception step, the aircraft is designed by experts so that the wings support a given nominal load envelope, dictated by physical

considerations such as desired aircraft manoeuvrability, gust, and many other manufacturing constraints. The larger the supported loads are, the larger the structural stiffeners and mass reinforcements should be. The aircraft mass is consequently bigger and its consumption during flight increased. In this context, gust load alleviation (**GLA**) control function plays an important role in the aircraft conception: it is aimed at lowering the loads envelope and thus at reducing the aircraft overall mass, consumption and emissions (see [50] for details). To achieve this **GLA** function, as illustrated in Figure 6, model-based control design approaches are usually preferred. In this section, following [50], we illustrate through a generic business jet aircraft model constructed by Dassault-Aviation, how the Loewner framework is a pivotal tool used in the industry to simplify the complexity of these dynamical models, prior control design and analysis.

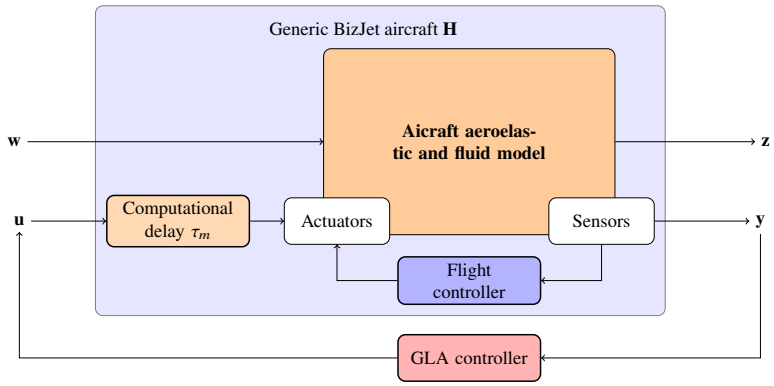

Figure 6: Closed-loop architecture of the **GLA** problem. The complete aeroservoelastic dynamical aircraft model **H** includes the "Flight controller", "Actuators", "Sensors" and "Computational delay τ_m". The "GLA controller" is **GLA** function to be computed. Signals **w**, **u**, **z** and **y** denote the exogenous inputs, control inputs, performance outputs and measurements, respectively. Then h denotes the sampling time for the **GLA**.

At each flight and mass configuration, a gust load oriented linear dynamical model considering aerodynamical, structural and actuator dynamics is constructed. Generic aircraft models have the following continuous-time realization

$$\mathcal{S}: \begin{cases} \mathbf{E}\mathbf{x}(t) = \mathbf{A}_0\mathbf{x}(t) + \mathbf{A}_1\mathbf{x}(t-\tau_1) + \mathbf{A}_2\mathbf{x}(t-\tau_2) + \mathbf{B}_u\mathbf{u}(t) + \mathbf{B}_w\mathbf{w}(t)\ , \\ \mathbf{y}(t) = \mathbf{C}_0\mathbf{x}(t) + \mathbf{C}_1\mathbf{x}(t-\tau_m) \text{ where }, \\ \mathbf{E}, \mathbf{A}_0, \mathbf{A}_1, \mathbf{A}_2 \in \mathbb{R}^{n\times n}, \mathbf{B}_u \in \mathbb{R}^{n\times n_u}, \mathbf{B}_w \in \mathbb{R}^{n\times n_w}, \mathbf{C}_0, \mathbf{C}_1 \in \mathbb{R}^{p\times n}. \end{cases} \tag{56}$$

where $\mathbf{x}(t) \in \mathbb{R}^n$, $\mathbf{u}(t) \in \mathbb{R}^{n_u}$, $\mathbf{w}(t) \in \mathbb{R}^{n_w}$ ($m = n_u + n_w$) and $\mathbf{y}(t) \in \mathbb{R}^p$ are the internal variables, control input, exogenous gust input and output signals, respectively. In the considered case, $n_u = 3$, $n_w = 1$ ($m = 4$), $p = 5$ and $n \approx 500$. The presence of internal delays is caused by the physical restitution of the gust impact over the fuselage at three different locations which are function of the aircraft velocity. Moreover, due to the model construction method (see *e.g.* [51] or [50]), the $\mathbf{E}$ matrix may also be rank deficient. Here, due to the additional double derivative and delay structure added to accurately describe the gust disturbance effect along the fuselage, $\mathbf{rank}\,\mathbf{E} = n - 6$. Following (56), the gust load model transfer associated function $\mathbf{H}$, from $[\mathbf{u}^T, \mathbf{w}^T]^T$ to $\mathbf{y}$ thus reads,

$$\mathbf{H}(s) = \left(\mathbf{C}_0 + \mathbf{C}_1 e^{-\tau_m s}\right)\left(s\mathbf{E} - \mathbf{A}_0 - \mathbf{A}_1 e^{\tau_1 s} - \mathbf{A}_2 e^{\tau_2 s}\right)^{-1}\mathbf{B} \in \mathbb{C}^{p\times m} \tag{57}$$

We seek a simplified rational model description to be used in place of (57) for fast simulation, control design and (modal) analysis while avoiding dealing with an infinite number of eigenvalues and transcendental equations related to the resolvant $\mathbf{\Phi}(s) = \left(s\mathbf{E} - \mathbf{A}_0 - \mathbf{A}_1 e^{\tau_1 s} - \mathbf{A}_2 e^{\tau_2 s}\right)^{-1}$. The first step in the process consists in gridding the interpolation (support points) along the imaginary axis and collecting the associated response as follows (with $\overline{n} = \underline{n} = n = 500$, $2n = N$ and $\omega_i \neq \omega_j$):

$$\begin{aligned} \{z_k\}_{k=1}^N &= \{\imath\omega_i, -\imath\omega_i\}_{i=1}^{n/2} \cup \{\imath\omega_j, -\imath\omega_j\}_{j=1}^{n/2} \text{ and} \\ \{\Phi_k\}_{k=1}^N &= \{\Phi_i, -\overline{\Phi_i}\}_{i=1}^{n/2} \cup \{\Phi_j, -\overline{\Phi_j}\}_{j=1}^{n}. \end{aligned} \tag{58}$$

where $\omega_i, \omega_j \in \mathbb{R}_+$ are the frequencies at which one evaluates each transfer $\mathbf{H}$. In our application ω_i and ω_j are selected to be logarithmically spaced.

Remark 4 (About a Padé delay approximation) *One option is to replace the delays with a Padé approximation, which preserves the gain but modifies the phase. While this is classically used in many applications, it is, to the authors experience, not the most accurate way to deal with internal and external delays. Indeed, Padé often results in significant error in the phase, which can be inappropriate for flexible structures. In addition, the use of Padé will drastically increase the model internal dimension which in turn is not appropriate for model reduction. Therefore, the accuracy / complexity ratio is not in favour of Padé approximation (see also Figure 7).*

Figure 7 illustrates the transfer function from the gust disturbance to a wing bending moment output, used to monitor the gust envelope. It compares the responses of the original irrational model $\mathbf{H}$ with its rational approximate $\mathbf{H}_n$ constructed with Loewner and its rational approximation $\mathbf{H}_{\text{Padé}}$ obtained with Padé.

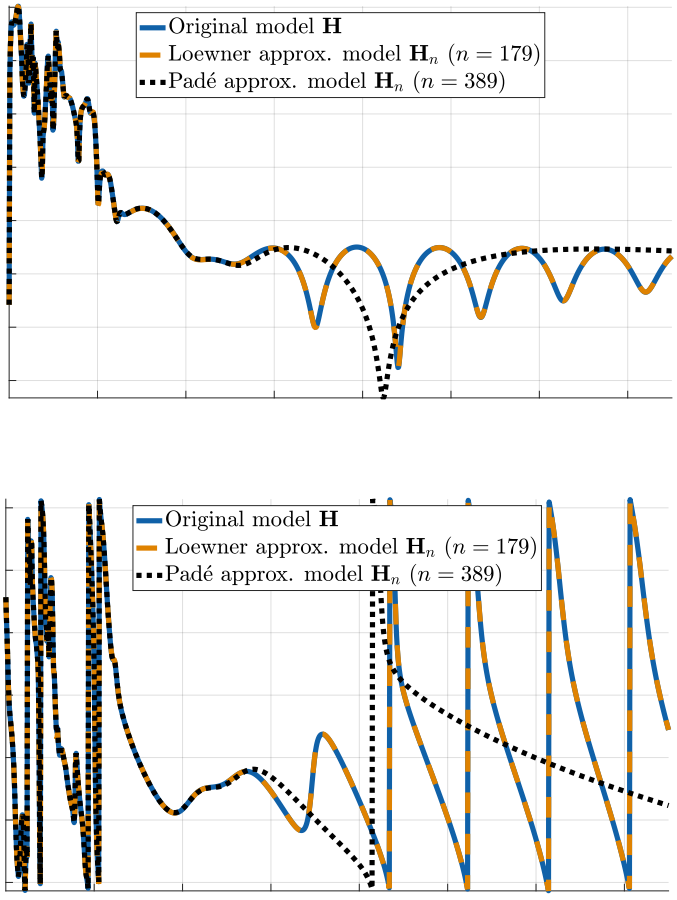

Figure 7: Top: frequency response gain (left) and impulse response (right). Bottom: frequency phase response. Comparison of the original model with the rational approximation obtained by Loewner interpolation and Padé.

Figure 7 emphasises the good performance of the rational model obtained by Loewner after reducing the complexity of the model (internal variable reduced). Most interestingly, the phase is much well captured by the Loewner approach than with Padé, using even less internal variables. In [50], this rational model is then used for frequency-limited reduction and **GLA** controller synthesis, leading to an impressive load envelope

reduction which is not achievable without the use of a Loewner interpolatory approach. This result emphasizes the importance of the Loewner framework for aircraft consumption reduction objective.

3.2 Ground vibration tests on Business jet aircraft

We continue on the business aircraft benchmark provided by Dassault-Aviation. Now we move from the gust load problem to the vibration one. While the former is more related to (the low frequency) structure and consumption issues, the latter is related to (the medium frequency) fatigue and comfort issues. Anti-vibration controllers are usually designed using model-based approaches in order to reduce the undesirable amplifications of the aerodynamical effects on the fuselage around some specified frequencies (see [48] for details). After such a model-based design and validation step, Ground Vibration Tests (**GVT**) are performed to validate the control performance, but also to validate the model.

The benchmark considered here illustrates the generic business jet **GVT**, performed on a Falcon 7X at Istres, France, in 2015 [40, 41][6]. The first step consists in designing an anti-vibration controller aimed at attenuating the vibrations at the passenger cabin and specified fatigue locations in response to aerodynamics turbulence occurring at specified frequencies. At the next step Dassault-Aviation engineers implemented the control law on the real business jet aircraft. Then, using shakers applied at some aircraft locations, the structure was excited, thus simulating aerodynamic disturbances. Hundreds of sensors were positioned on the aircraft and used for analysis[7]. Figure 8 (top) shows the frequency response of the data collected from a single-input and 100-outputs; this is compared with the frequency response of a rational model of minimal complexity constructed, in open loop *e.g.* without anti-vibration devices. The singular values drop is also illustrated in Figure 8 (bottom). In both cases, the truncation and rank computation are performed via **SVD**[8].

[6] Flight test have been performed in 2017, validating the results.

[7] https://drive.google.com/file/d/1H2GqlYkiny_PZND2ekB6swSetoGcmFTK/view shows a video that illustrates the kinematic effect of the control law acting on the tail surface to reduce the vibrations.

[8] Notice that other methods can be considered such as **CUR**, **EV**, see *e.g.* [33].

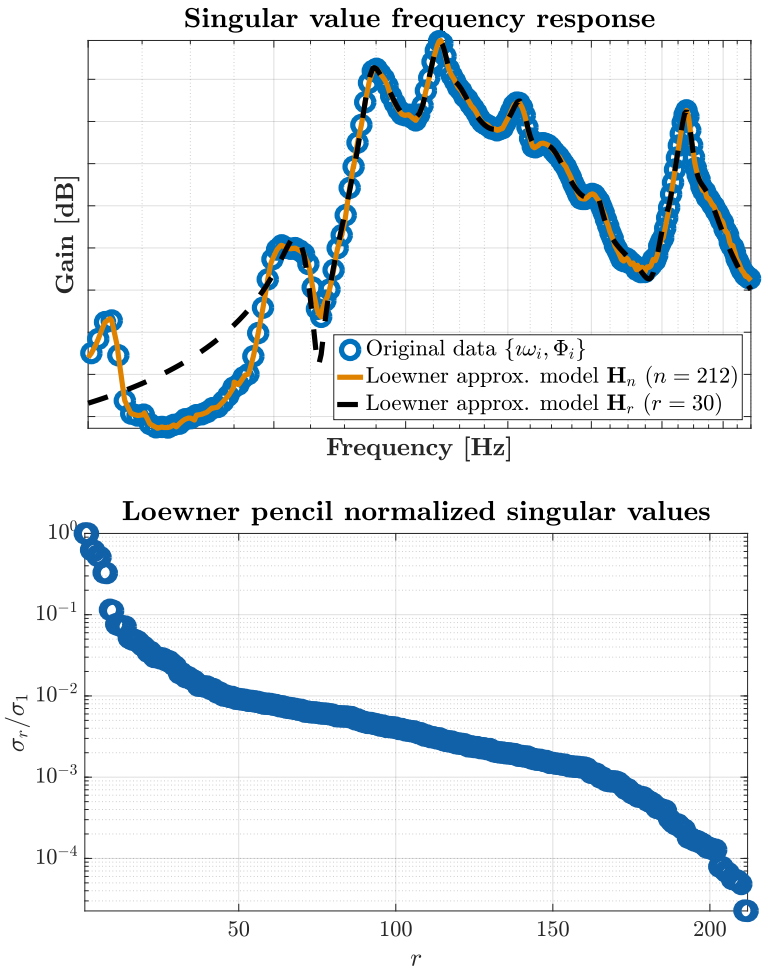

Figure 8: Top: singular value frequency response of the data (blue circles) the minimal Mc Millan degree rational function (solid orange) and reduced 30-th order rational model (dashed black). Bottom: singular values drop of the Loewner pencil.

Additional information may be found in [40, 41] or in §2.4.7 of [44]. In this industrial challenging case, one important feature of the Loewner framework illustrated here is to be able to recover the transfer function from raw data, and perform modal (residue) analysis. In the considered industrial application, such a feature allows engineers to re-adjust the theoretical models accordingly to the collected real data, detect some new phenomena and re-adjust the control law. This step contributes to the quest for a so-called *digital twin*.

3.3 Hydroeletricity open-channel benchmark

In this third example, we consider a model representing the level h of an open-channel as a function of the inflow q_i and outflow q_o inputs. Such a model is used by hydro-electricity engineers from Electricité De France to monitor the level of a river in order to control the available energy (note that in real applications, these model come in a network). One important feature of open-channels is that they can be viewed as easily available energy tanks. Indeed, unlike windmills or nuclear factories, energy is available on demand, and unlike solar panels, energy (water) can be stored. In France, in May 2021, the hydraulic energy represented about 10% of the total produced energy[9]. Well understanding the underlying dynamics in view of energy management is therefore crucial in the global warming frame.

[9] https://www.rte-france.com/eco2mix/la-production-delectricite-par-filiere.

Mathematically such models for such benchmarks belong to the class of linear partial differential equations (**PDE**). Such a models come from the so-called Saint-Venant equations, used to model the dynamics of open channel flow (see [19] for a detailed description). They consist of two nonlinear hyperbolic **PDE**s. For a channel of length L and bottom slope I, we have

$$\begin{array}{rcll} \dfrac{\partial S}{\partial t} + \dfrac{\partial Q}{\partial x} & = & 0 & \text{(mass conservation)} \\ \dfrac{\partial Q}{\partial t} + \dfrac{\partial (Q^2/S)}{\partial x} + gS\dfrac{\partial H}{\partial x} & = & gS(I-J) & \text{(momentum conservation),} \end{array} \tag{59}$$

where $x \in [0, L]$ is the spatial variable, t the time variable, $H(x,t)$ the water depth, $S(x,t)$ the wetted area, $Q(x,t)$ the discharge, g the gravity acceleration and J the Manning-Strickler friction[10].

These equations are quite complex to simulate and analyse. Under mild assumptions a linearization around an equilibrium point (Q_0, H_0), detailed in [19], expresses the variation relations (q, h), between inflow (q_e, being q at $x = 0$), outflow (q_s, being q at $x = L$) and the water depth (h, at a given measurement point x) as follows,

$$h(x,s) = \mathbf{G}_e(x,s)q_e(s) - \mathbf{G}_s(x,s)q_s(s), \tag{60}$$

where

$$\begin{array}{rcl} \mathbf{G}_i(x,s) & = & \dfrac{\lambda_1(s)e^{\lambda_2(s)L+\lambda_1(s)x} - \lambda_2(s)e^{\lambda_1(s)L+\lambda_2(s)x}}{B_0 s(e^{\lambda_1(s)L} - e^{\lambda_2(s)L})} \text{ and} \\ \mathbf{G}_o(x,s) & = & \dfrac{\lambda_1(s)e^{\lambda_1(s)x} - \lambda_2(s)e^{\lambda_2(s)x}}{B_0 s(e^{\lambda_1(s)L} - e^{\lambda_2(s)L})}. \end{array} \tag{61}$$

Clearly $\mathbf{G}_i$ and $\mathbf{G}_o$ yield a non-rational infinite dimensional model. For a frozen measurement point $x = x_m$, then one has

$$h_{x_m}(s) = \mathbf{H}(s)\mathbf{u}(s) = \mathbf{G}_i(x_m, s)q_i(s) + \mathbf{G}_o(x_m, s)q_o(s). \tag{62}$$

where $\mathbf{u}(s)$ contains the two inputs $q_i(s)$ and $q_o(s)$ and where $\mathbf{H}$ is now a one output two inputs complex-valued transfer function. Figure 9 illustrates the approximation features and accurate reconstruction of the open-channel phenomenon. To obtain this result, we consider complex conjugated points $\{z_k\}_{k=1}^{N} = \{\imath\omega_k, -\imath\omega_k\}_{k=1}^{N/2}$ (where $\overline{n} = \underline{n} = 300 = N/2$) sampled between 10^{-4} and $10^{1.5}$ in logarithmic space. Then, the responses

$$\mathbf{H}(s) \text{ and } \widetilde{\mathbf{H}}(s) = \mathbf{H}(s)\frac{s}{(s+10^{-2})(s+10^{-3})}, \tag{63}$$

are computed. Dealing with $\mathbf{H}$ remains standard with the framework presented so far. By approximating $\widetilde{\mathbf{H}}$ removes the integral action and enforces roll-off in high frequency, and thus allows to deal with limited energy functions ($\widetilde{\mathbf{H}} \in \mathcal{H}_2$). Therefore, the resulting interpolated model should be post processed as $\widetilde{\mathbf{H}}_n \leftarrow \mathbf{H}_n \frac{(s+10^{-2})(s+10^{-3})}{s}$ to recover the original one.

[10] Numerical values of this model are provided at https://morwiki.mpi-magdeburg.mpg.de/morwiki/index.php/Hydro-Electric_Open_Channel

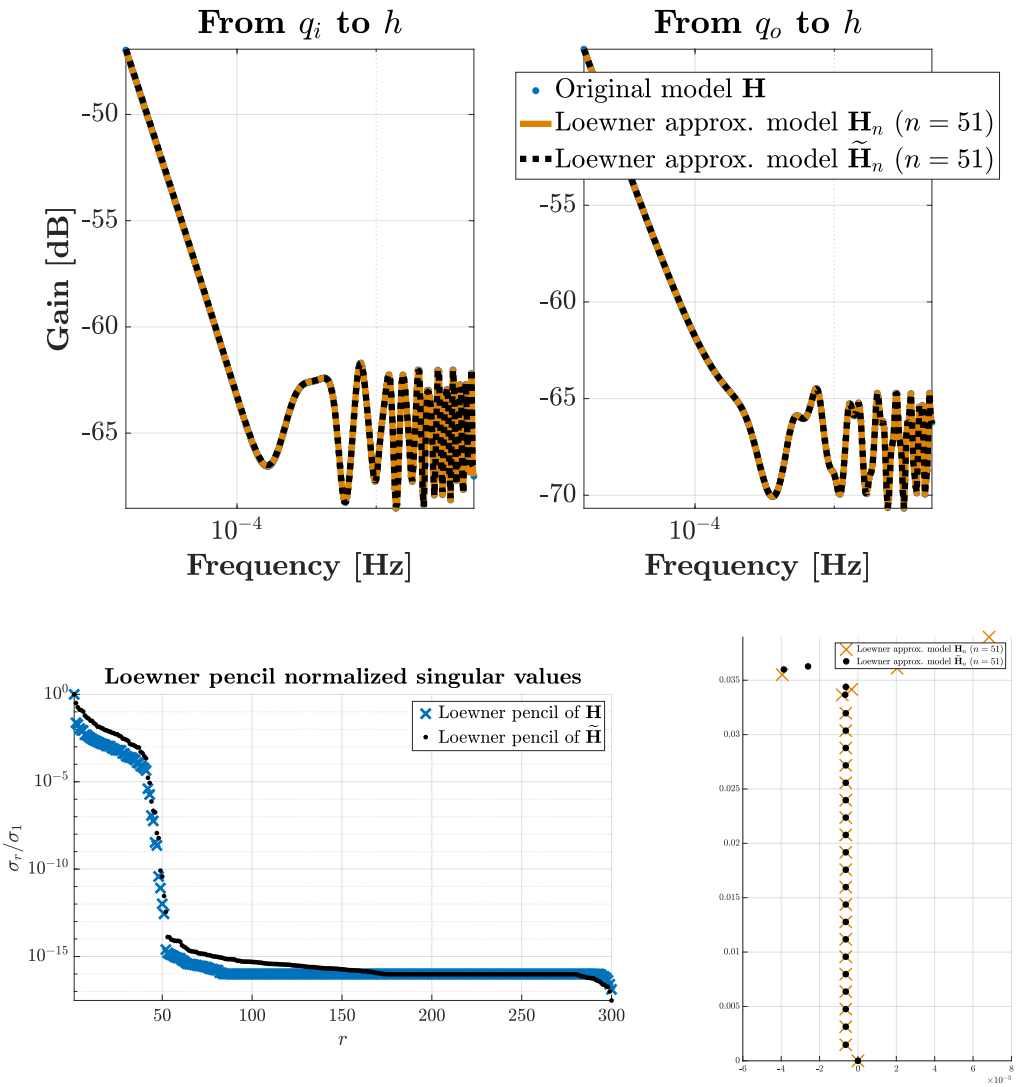

Figure 9: Top: frequency response comparison between the original irrational model an two approximated Loewner models. Bottom left: Singular values drop of the Loewner pencil for the two models. Bottom right: eigenvalues of the resulting minimal order rational approximation.

As illustrated on Figure 9, both approaches lead to a perfect matching of the irrational transfer. Interestingly, working with $\widetilde{\mathbf{H}}$ instead of $\mathbf{H}$ leads to a model with all singularities on the left hand side plus the 0 one. Working with the shifted function $\widetilde{\mathbf{H}}$ illustrates how one can perform grey box identification by simply shifting the original data. Here, the integral action (physically known from open-channel models) is removed and added afterward. The trick of working with $\mathcal{H}_2$ functions instead of $\mathcal{H}_\infty$ ones (as $\mathbf{H}$ is) is more numerical than theoretical as is avoids bad conditioning of exact 0 singularities and focusing on low dynamics first. Moreover, in the similar flavour, one may also remove the delay part of such a transfer by pre-multiplying by $e^{s\tau}$, where $\tau \in \mathbb{R}_+$ is the estimated delay of the function, and thus dealing with $\widetilde{\mathbf{H}}(s) = \mathbf{H}(s)\dfrac{se^{s\tau}}{(s+10^{-2})(s+10^{-3})}$ instead. This feature is relevant for real-life applications.

4 Control in the Loewner framework

Let us now deviate from the original purpose of the Loewner framework, initially introduced to provide solutions to the identification, approximation and reduction problems through the lens of rational function construction. Here instead, such a framework is used for feedback controller design. More specifically it is used as in some traditional loop shaping methods, to fit a reference controller [20,22,39,57]. However, in the proposed setup, the reference controller is not computed by means of a model but rather involving input-output data of the system.

4.1 Data-driven control, virtual reference model and Loewner framework

In this section, the Loewner framework will be used for synthesizing a controller directly from measured data. Hence, this a data-driven control (**DDC**) framework[11]. Data-driven control consists in recasting the control design problem as an identification one. Major advantages of this strategy are: *(i)* it provides a controller tailored to the actual system and *(ii)* that is not dependent of the underlying mathematical model description. This change of paradigm shifts the model identification / simplification process to the controller directly.

The considered technique belongs to the so-called *reference model approaches* and more specifically relies on the definition of a so-called *ideal controller*, derived from a reference model. Recently [35, 55] moved the formulation in the frequency-domain, with the use of the Loewner framework as the identification tool, allowing to skip the controller complexity selection thanks to its rank properties (see section 2). The Loewner data-driven control (**L-DDC**) is thus a combination of determining the ideal controller from frequency-domain data via a reference model and the use of the Loewner framework [38] to construct a reduced order controller. Such an interpolatory-based data-driven control design solves problems faced by practitioners: *(i)* the controller design is directly obtained using open-loop raw data collected on the experimental setup, *(ii)* without any prior controller structure or order specification. This approach has proven to be effective on infinite dimensional systems [28], for digital control [55], experimental application [45] and relates to data-driven stability analysis [46].

4.2 The L-DDC rationale at a glance

The **L-DDC** procedure boils down to two steps: first deriving the *ideal controller* definition and second the *controller identification* via interpolation in the Loewner framework (in [28] the use of Loewner in this context is compared with **AAA** and **VF**). We recall the mains steps in the **SISO** case. Following Figure 10, the objective is to find a controller $\mathbf{K} \in \mathbb{C}$ that minimizes the difference between the resulting closed-loop and a given user-defined reference model $\mathbf{M} \in \mathbb{C}$. This is made possible through the definition of the ideal controller $\mathbf{K}^\star$, being the **LTI** controller that would have given the desired reference model behaviour if inserted in the closed-loop. The latter is defined as $\mathbf{K}^\star = \mathbf{H}^{-1}\mathbf{M}(I-\mathbf{M})^{-1}$. In the data-driven case, this definition may be recast as a discrete set of equations (where $\{z_k\}_{k=1}^N \in \mathbb{C}$, $k = 1, \ldots, N$)

$$\mathbf{K}^\star(z_k) = \mathbf{H}(z_k)^{-1}\mathbf{M}(z_k)(I - \mathbf{M}(z_k))^{-1}, \tag{64}$$

where $\mathbf{H}(z_k)$ is the evaluation of the considered model, if available. In an experimental context, one usually considers sampling $\mathbf{H}$ at $z_k = \imath\omega_k$ ($\omega_k \in \mathbb{R}_+$). In this case input-output measurements are given as $\mathbf{H}(\imath\omega_k) = \overline{\mathbf{y}}(\imath\omega_k)/\overline{\mathbf{u}}(\imath\omega_k)$, where $\overline{\mathbf{u}}$ and $\overline{\mathbf{y}}$ are the Fourier transform of $\mathbf{u}$ and $\mathbf{y}$, respectively. Finding a controller $\mathbf{K}$ that fits $\mathbf{K}^\star(z_k)$ can be considered to be an identification problem. Thus, in the Loewner framework, the control design boils down to finding a rational function $\mathbf{K}$ interpolating (64).

[11] The reader may notice that **DDC** methods have a long history dating to the proportional, integral, derivative (**PID**) tuning method by Ziegler-Nichols in early 40's or the self tuning regulator by Åström in the 90's (see *e.g.* §3 of [34] for more details and references).

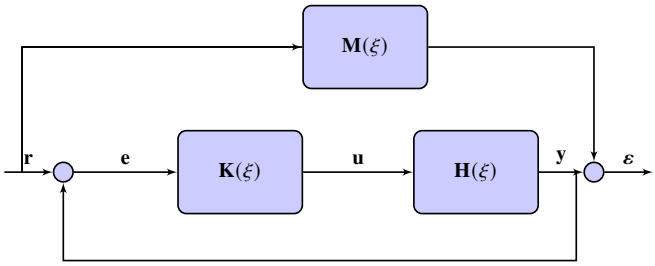

Figure 10: Data-driven control problem formulation: **M** is the reference model (objective) and **K** the controller to be designed.

In what follows, two **L-DDC** applications are illustrated. The first one involves experimental data and considers the design of a reference tracking controller applied on a pulsed fluidic actuator (in short, **PFA**), see section 4.3, [45]). The second case considers a numerical benchmark representing the boundary control a wave equation, described by an infinite dimensional equation. For this latter case, equivalence with a model-based approach is also illustrated (see also [46]).

4.3 Pulsed fluidic actuator

The design of active closed-loop flow controllers constitutes an important field of research in fluid mechanics (see *e.g.* [53, 56]). The possible objectives are to maintain laminarity or delay transition to turbulence, decrease turbulence level, reduce noise, increase lift and decrease drag, enhance mixing and heat release, etc. Without detailing the methodology employed in each case, in most cases, both the sensor(s) and the actuator(s) are supposed to be lumped and ideal (*i.e.* sensors deliver instantaneous accurate measurements and actuators deliver the exact control signals with no delay, no noise, continuous control signal and unbounded intervals). These developments are relevant for academic and methodological purposes. However, to move towards experimental applications and real-life validations, it is essential to consider realistic set-ups. Considering the actuator-sensor combination is necessary and is the core contribution of [45], where the **L-DDC** is applied on a **PFA**. **PFA** are on/off actuators that blow air to modify the pressure in a flow setup. They are typically used to control fluidic phenomena. The control setup considered is schematized on Figure 11

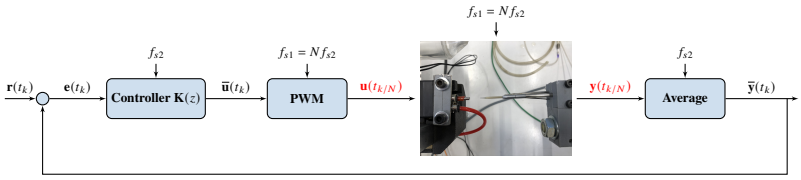

Figure 11: **PFA** control setup. **Controller** $\mathbf{K}(z)$ is the sampled-time control law to be computed (sampled at f_{s2}), Pulsed Width Modulation (**PWM**) block transforms the continuous signal into on/off values (sampled at frequency f_{s1}) and **Average** block is a down-sampling function providing the mean value of the input signal. The system is illustrated by its top view photo, where the left side represents the **PFA** and the right side, the Pressure Sensor (**PS**).

After exciting the **PFA** using a pseudo random binary sequence $\mathbf{u}(t_{k/n})$, output data $\mathbf{y}(t_{k/n})$ are collected. The corresponding frequency responses $\bar{\mathbf{u}}$ and $\bar{\mathbf{y}}$ are computed and transfer function values $\mathbf{H}(\imath\omega_k)$ are thus obtained. Applying (64) with $z_k = \imath\omega_k$ and the Loewner approach, it leads to a singular value decay indicating that a first or third order model is sufficient to recover the main dynamics (see Figure 12).

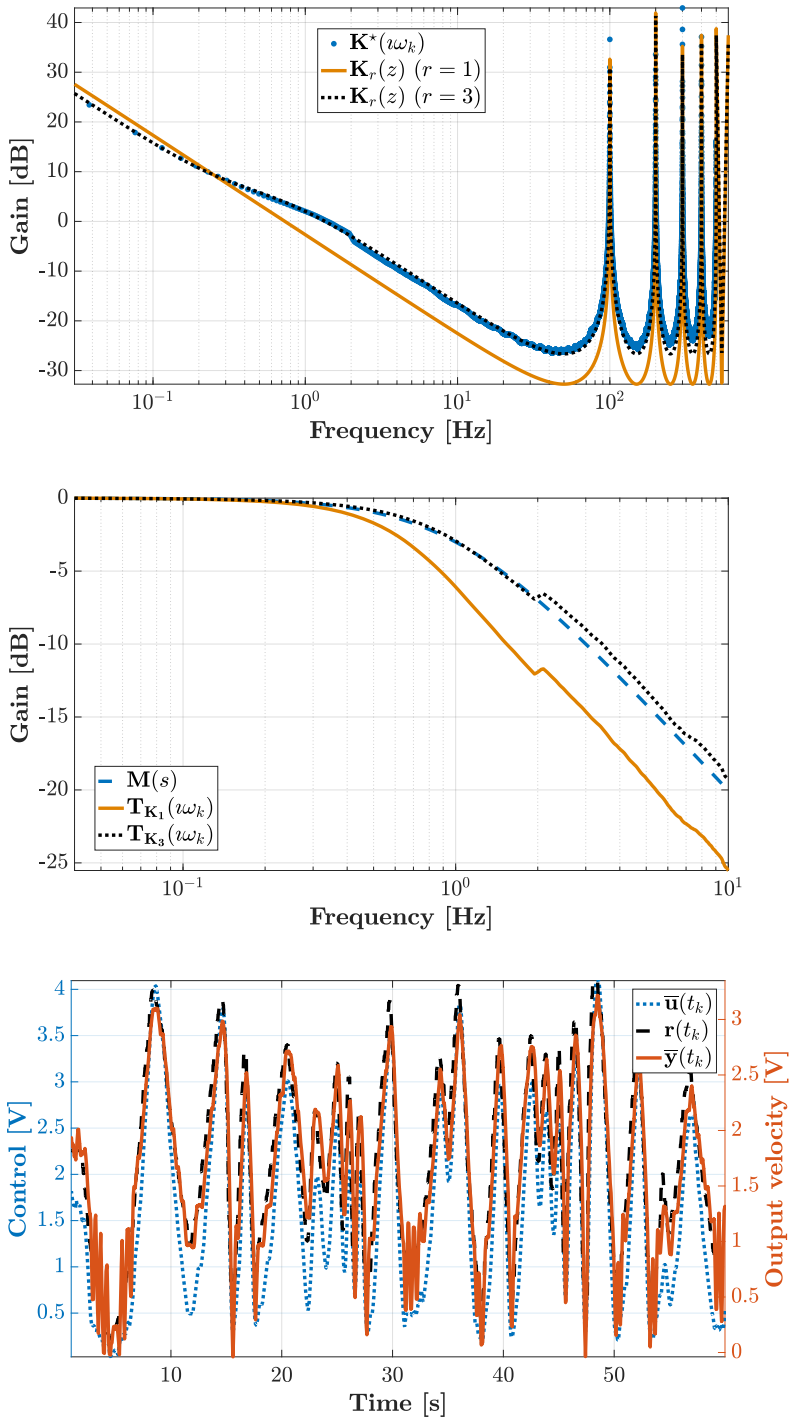

Figure 12: Top: gain of the frequency responses of the ideal controller $\mathbf{K}^\star$ evaluated at the available frequencies (blue dots) an of the estimated controller $\tilde{\mathbf{K}}_\mathbf{r}(s)$ of order $r = 1$ (solid orange) and $r = 3$ (dotted black). Middle: closed-loop response estimation using controller $\mathbf{K_1}$ and $\mathbf{K_3}$ of the averaged output $\overline{\mathbf{y}}(t_k)$ (solid orange an dotted black) based on the measured data. Time-domain response to a variable reference trajectory $\mathbf{r}(t_k)$ (dashed black), averaged control signal $\overline{\mathbf{u}}(t_k)$ (dotted blue) and averaged output (solid orange).

One important result is the ability of the **L-DDC** to construct, directly from raw open-loop data, a control law performing well on an experimental setup. Relevant in this context is that the **L-DDC** structure and complexity is almost automatically chosen by the Loewner framework, and no pole pre-assignment is required.

4.4 Transport phenomena benchmark

Finally, let us consider the case of a one dimensional transport equation controlled at its left boundary through a second order actuator. This model is used in [46] or [28] and detailed in §2, Example 7 of [44]. This phenomenon is represented by a linear **PDE** with constant coefficients interconnected with a second order linear **ODE** actuator, as described in (65).

$$\begin{aligned} \frac{\partial \tilde{y}(x,t)}{\partial x} + 2x\frac{\partial \tilde{y}(x,t)}{\partial t} &= 0 && \text{(transport equation)} \\ \tilde{y}(x,0) &= 0 && \text{(initial condition)} \\ \tilde{y}(0,t) &= \frac{1}{\sqrt{t}}\tilde{u}_f(0,t) && \text{(boundary control input)} \\ \frac{\omega_0^2}{s^2+m\omega_0 s+\omega_0^2}u(0,s) &= u_f(0,s) && \text{(actuator model),} \end{aligned} \tag{65}$$

where $x \in [0\ L]$ ($L = 3$) is the spatial variable. Then, $\omega_0 = 3$ and $m = 0.5$ are the input actuator parameters. The scalar input of the model is the vertical force applied at the left boundary, *i.e.* at $x = 0$. We denote the input $\tilde{\mathbf{u}}(0,t)$ in the time-domain or $\mathbf{u}(0,s)$ in the complex one. Similarly, the output at location x is given as $\tilde{\mathbf{y}}(x,t)$ for the time-domain and $\mathbf{y}(x,s)$ in the complex one. Such a transport equation set may be used to represent a simplified one dimensional wave equation used in telecommunications, traffic jams prediction, *etc*.

By applying the Laplace transform, one obtains the transfer function from the input $\mathbf{u}(0,s)$ to the output $\mathbf{y}(x,s)$:

$$\mathbf{y}(x,s) = \frac{\sqrt{\pi}}{\sqrt{s}}e^{-x^2 s}\frac{\omega_0^2}{s^2+m\omega_0 s+\omega_0^2}\mathbf{u}(0,s) = \mathbf{G}(x,s)u(0,s). \tag{66}$$

Relation (66) links the (left boundary) input to the output through an irrational transfer function $\mathbf{G}(x,s)$ for any value x[12]. Let us now consider that one single sensor is available and is located at $x_m = 1.9592$ along the x-axis[13]. The transfer from the same input $\mathbf{u}(0,s)$, denoted by $\mathbf{u}(s)$ to $\mathbf{y}(x_m,s)$ denoted by $\mathbf{y}(s)$ then reads $\mathbf{y}(s) = \mathbf{y}(x_m,s) = \mathbf{G}(s,x_m)\mathbf{u}(0,s) = \mathbf{H}(s)\mathbf{u}(s)$, where $\mathbf{H}(s)$ is now a **SISO** complex-valued irrational transfer function.

4.4.1 A model-driven approximation and control

By Loewner interpolation, the transfer function $\mathbf{H}$ can be approximated by a rational function $\mathbf{H}_r$ ($r = 33$). Then, standard feedback synthesis methods can be applied. In this example, the HINFSTRUCT function (embedded in the MATLAB Robust Control Toolbox) has been used [12]. It allows designing fixed structure controllers while minimising some $\mathcal{H}_\infty$-norm oriented performance criterion. Starting from $\mathbf{H}_r$, let us first define the following generalised plant $\mathbf{T} = \mathbf{H}_r\mathbf{W}_o$, where $\mathbf{W}_o$ is the weighting filter defining the output signals on which the $\mathcal{H}_\infty$-norm optimisation will be performed. $\mathbf{W}_o$ is constructed to define the desired closed-loop performances attenuation and its bandwidth which share a similar architecture as the one on Figure 10. Using the same notation, the performance transfer from $\mathbf{r}$ to $\mathbf{e}$, is defined as $\mathbf{T_{re}} = \mathbf{H}_r\mathbf{W}_o$. In the case considered, one aims at tracking the reference signal $\mathbf{r}$ and limiting the control action $\mathbf{u}$. One can then construct $W_o = \mathbf{blkdiag}(W_e, W_u) = \mathbf{blkdiag}(10\frac{s+1}{s}, \frac{s+10}{s+1000})$ describing performance output $\mathbf{z} = \mathbf{blkdiag}(W_e\mathbf{e}, W_u\mathbf{u})$. The W_e weighting filter has been chosen to weight the sensitivity function and guarantee no steady-state error (*e.g.* roll-off in low frequencies) and a bandwidth around 10^{-1} rad/s. W_u is used to weigh the actuator action in high

[12] Interestingly, the exact time-domain solution of (65), along x, is given by $\tilde{\mathbf{y}}(x,t) = \tilde{u}_f^{t-x^2}/\sqrt{t}$, where $\tilde{\mathbf{u}}_f$ is the output of the second order actuator transfer function, in response to u.

[13] In the rest of the chapter, x will be discretized with 50 points from 0 to $L = 3$, and x_m has been chosen to be located at $x(\lfloor 50 \times 2/3 \rfloor)$.

frequencies (here the actuator will roll-off above 10rad/s). Notice that this is also a fairly standard way of weight selection. The $\mathcal{H}_\infty$ control design consists in finding the controller $\mathbf{K}$, mapping $\mathbf{e}$ to $\mathbf{u}$, such that, $\mathbf{K} := \arg\min_{\tilde{\mathbf{K}}\in\mathcal{K}} ||\mathcal{F}_l(\mathbf{T_{rz}}, \tilde{\mathbf{K}})||_{\mathcal{H}_\infty}$, where $\mathcal{F}_l(\cdot,\cdot)$ is the lower fractional operator defined as (for appropriate partitions of M and K) by $\mathcal{F}_l(M,K) = M_{11} + M_{12}K(I - M_{22}K)^{-1}M_{21}$ [37]. Moreover, it is possible to define the class $\mathcal{K}$ of $\mathbf{K}$ to be restricted to the filtered proportional integral (**PI**), meaning that one is seeking $\mathbf{K}$ with the following form, $\mathbf{K}(s) = (k_p + k_i\frac{1}{s})\frac{1}{s/a+1}$, where $k_p, k_i, a \in \mathbb{R}$. After optimisation, one obtains $k_p = 0.1914$, $k_i = 0.0251$ and $a = 5667.2$ (note also that in this case, the optimal attenuation reached is $\gamma_\infty = 66.9558$) [14].

4.4.2 Data-driven control

Let us now apply the **L-DDC** rationale, instead of a model based control design. As explained in §6.1-6.2 of [34], the reference model choice is a key factor for the **L-DDC** success, as for any other model reference control procedure. Indeed, the latter should not only represent a desirable closed-loop behaviour, but also achievable dynamics of the considered system (*i.e.* the ideal controller should not internally destabilise the plant). A reference model is said to be achievable by the plant if the corresponding ideal controller internally stabilises the plant. Here let us skip this point and focus on the equivalence of model vs. data-based design. Let the reference model $\mathbf{M}$ be the closed-loop rational function obtained by the previous approach interconnecting $\mathbf{H}_r$ with the obtained filtered **PI** control law obtained in the above section.

By computing the ideal controller through (64), we again compute the Loewner pencil, leading to a minimal realization with $n = 42$. Obviously, such a control order is prohibitive for classical control applications. The singular values decay indicates that an order $r = 2$ is enough to catch the main dynamics of the underlying controller. One obtains $\mathbf{K}_r$ ($r = 2$) with transfer function

$$\mathbf{K}_2(s) = \frac{1082.7(s + 0.1313)}{s(s + 5656)}, \tag{67}$$

being very close to the numbers obtained by the model-based approach[15]. The controller and resulting close-loop frequency response gains are illustrated on Figure 13.

[14] The optimisation is done using the HINFSTRUCT routine, allowing minimising the closed-loop interconnection of $\mathbf{T_{rz}}$ with $\tilde{\mathbf{K}}$. In general, we seek for $||\mathcal{F}_l(\mathbf{T_{rz}}, \mathbf{K})||_{\mathcal{H}_\infty} = \gamma_\infty \leq 1$. Here, we simply aim to reaching stability and tracking performances.

[15] The model based approach yield to $\frac{1084.9(s+0.1313)}{s(s+5667)}$

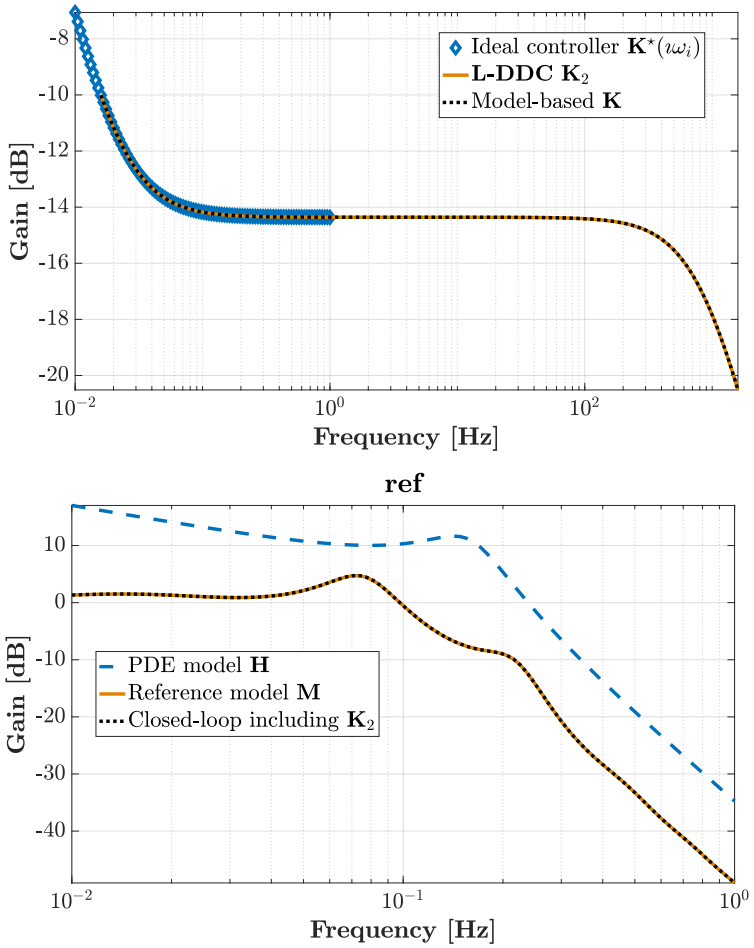

Figure 13: Top: frequency response of the controller (ideal, model-based and data-driven). Bottom: open-loop vs. closed-loop frequency responses.

Interestingly, with reference to Figure 13, $\mathbf{K}_r$ perfectly recovers the model-based requested performances of $\mathbf{M}$ with a controller of rational order two (indeed, we expected to observe this result since we knew from the model-based approach presented in Section 4.4.1 that a rational control of order leading to this performance is achievable).

This example demonstrates how the Loewner framework can be effectively used, either for model-based, or for data-driven control. Interestingly, by choosing the closed-loop performances $\mathbf{M}$ obtained with the model-based approach, the controller $\mathbf{K}_r$ exactly recovers the original properties, while skipping the model construction step and the order selection. This property reduces the model construction step and allows a quick design of the controller. However, this main advantage is balanced by the fact that in the model-based approach, the stability assessment is usually carried out using the approximate model, here $\mathbf{H}_r$. The latter being very accurate, the eigenvalues computation is traditionally enough for concluding stability, robustness. On the contrary, in the second data-driven approach, stability cannot be analysed as easily. However, [46] suggests an approach based on the combination of Loewner with optimal $\mathcal{H}_\infty$ projections.

5 Summary and Conclusions

In this work, we have provided an inventory of selected extensions and applications of the Loewner framework. The main philosophy of this approach is as follows: use the available data to construct a model or a controller; if needed, apply compression techniques to reduce the complexity of the model or of the controller. The Loewner framework was shown to be applicable for reducing large-scale dynamical systems from computational fluid dynamics (such as the linearized Navier-Stokes model with more than half a million degrees of freedom), to data-driven modeling in aeronautics applications, and to various benchmarks described by complicated dynamics (characterized by irrational transfer functions, having multiple delays, with many input or output ports, with nonlinear terms etc.). The key observation here is that one can accomplish all of these successful endeavours by having access only to compressed data (transfer function measurements, Markov parameters, etc.), and nothing else. Moreover, the Loewner data-driven control approach was shown to faithfully recover the performance attained by other classical model-based control approaches. Thus, one advantage is the data-driven characteristic, and another is the robustness of the approach. The Loewner framework is hence a valid alternative to intrusive methodologies, and can be successfully used when data are available.

References

[1] A. C. Antoulas. *Approximation of large-scale dynamical systems*. SIAM, Philadelphia, 2005.

[2] A. C. Antoulas and B. D. O. Anderson. On the scalar rational interpolation problem. *IMA Journal of Mathematical Control and Information*, 3(2-3):61–88, 1986.

[3] A. C. Antoulas, C. A. Beattie, and S. Gugercin. *Interpolatory Methods for Model Reduction*. Society for Industrial and Applied Mathematics, Philadelphia, 2020.

[4] A. C. Antoulas, I. V. Gosea, and M. Heinkenschloss. On the Loewner framework for model reduction of Burgers' equation. In R. King, editor, *Active Flow and Combustion Control*, Notes on Numerical Fluid Mechanics and Multidisciplinary Design, pages 255–270. Springer, Cham, Switzerland, 2019.

[5] A. C. Antoulas, I. V. Gosea, and M. Heinkenschloss. Reduction of systems with polynomial nonlinearities in the Loewner framework. In *Book of Abstracts of XXI Householder Symposium on Numerical Linear Algebra, Selva di Fasano, Italy, June 14–19*, 2020.

[6] A. C. Antoulas, I. V. Gosea, and A. C. Ionita. Model reduction of bilinear systems in the Loewner framework. *SIAM Journal on Scientific Computing*, 38(5):B889–B916, 2016.

[7] A. C. Antoulas, S. Lefteriu, and A. C. Ionita. A tutorial introduction to the Loewner framework for model reduction. In *Model Reduction and Approximation*, chapter 8, pages 335–376. SIAM, 2017.

[8] A.C. Antoulas. The Loewner framework and transfer functions of singular/rectangular systems. *Applied Mathematics Letters*, 54:36–47, 2016.

[9] A.C. Antoulas, A.C. Ionita, and S. Lefteriu. On two-variable rational interpolation. *Linear Algebra and its Applications*, 436(8):2889–2915, 2012. Special Issue dedicated to Danny Sorensen's 65th birthday.

[10] A.C. Antoulas, S. Lefteriu, and A.C. Ionita. *Model reduction and approximation theory and algorithms*, chapter A tutorial introduction to the Loewner framework for model reduction. SIAM, Philadelphia. P. Benner, A. Cohen, M. Ohlberger and K. Willcox Eds, 2016.

[11] A.C. Antoulas, B. Zhu, Q. Zhang, B. York, B.W. O'Malley, and C. Dacso. A novel mathematical method for disclosing oscillations in gene transcription: A comparative study. *PLOS ONE*, 13(9):1–20, September 2018.

[12] P. Apkarian and D. Noll. Nonsmooth $\mathcal{H}_\infty$ Synthesis. *IEEE Transaction on Automatic Control*, 51(1):71–86, January 2006.

[13] A. Barbagallo, D. Sipp, and P.J. Schmid. Closed-loop control of an open cavity flow using reduced-order models. *Journal of Fluid Mechanics*, 641:1–50, 2008.

[14] P. Benner and T. Breiten. Interpolation-based $\mathcal{H}_2$-model reduction of bilinear control systems. *SIAM Journal on Matrix Analysis and Applications*, 33:859–885, 2012.

[15] P. Benner, S. Gugercin, and K. Willcox. A survey of projection-based model reduction methods for parametric dynamical systems. *SIAM Review*, 57(4):483–531, 2015.

[16] P. Benner, M. Ohlberger, A. Cohen, and K. Willcox. *Model Reduction and Approximation*. Society for Industrial and Applied Mathematics, Philadelphia, PA, 2017.

[17] T. Breiten and T. Damm. Krylov subspace methods for model order reduction of bilinear control systems. *Systems and Control Letters*, 59:443–450, 2010.

[18] T. Carleman. Application de la théories des équations intégrales linéaires aux systèmes d'équations différentielles non linéaires. *Acta. Math.*, 59:63–87, 1932.

[19] V. Dalmas, G. Robert, C. Poussot-Vassal, I. Pontes Duff, and C. Seren. From infinite dimensional modelling to parametric reduced order approximation: Application to open-channel flow for hydroelectricity. In *Proceedings of the 15th European Control Conference*, pages 1982–1987, Aalborg, Denmark, July 2016.

[20] J C. Doyle and G. Stein. Multivariable Feedback Design: Concepts for a Classical/Modern Synthesis. *IEEE Transaction on Automatic Control*, 26(1):4–16, 1981.

[21] G. Flagg and S. Gugercin. Multipoint Volterra series interpolation and $\mathcal{H}_2$ optimal model reduction of bilinear systems. *SIAM Journal on Matrix Analysis and Applications*, 36(2):549–579, 2015.

[22] B A. Francis and J C. Doyle. Linear Control Theory with an $\mathcal{H}_\infty$ Criterion. *SIAM Journal of Control and Optimization*, 25:815–844, 1987.

[23] K A. Gallivan, A. Vanderope, and P. Van Dooren. Model reduction of MIMO systems via tangential interpolation. *SIAM Journal of Matrix Analysis and Application*, 26(2):328–349, February 2004.

[24] I. V. Gosea and A. C. Antoulas. Model reduction of linear and nonlinear systems in the Loewner framework: A summary,. In *14th European Control Conference (ECC), July 15–17, Linz, Austria*, pages 345–349, 2015.

[25] I. V. Gosea and A. C. Antoulas. Data-driven model order reduction of quadratic-bilinear systems. *Numerical Linear Algebra with Applications*, 25(6):e2200, 2018.

[26] I. V. Gosea, D. S. Karachalios, and A. C. Antoulas. Learning reduced-order models of quadratic control systems from input-output data. e-print 2012.02075, arXiv, 2020. math.OC (accepted for publication at ECC21).

[27] I.V. Gosea. *Model order reduction of linear and nonlinear systems in the Loewner framework*. PhD thesis, Jacobs University Bremen, January 2017.

[28] I.V. Gosea, C. Poussot-Vassal, and A.C. Antoulas. On Loewner data-driven control for infinite-dimensional systems. In *Proceedings of the IEEE European Control Conference*, Virtual, June 2021.

[29] I.V. Gosea, Q. Zhang, and A.C. Antoulas. Preserving the DAE structure in the Lowner model reduction and identification framework. *Advanced Computing Mathematics*, 46(3), 2020.

[30] S. Gugercin, A C. Antoulas, and C A. Beattie. $\mathcal{H}_2$ Model Reduction for Large Scale Linear Dynamical Systems. *SIAM Journal on Matrix Analysis and Applications*, 30(2):609–638, June 2008.

[31] A C. Ionita and A C. Antoulas. *Matrix pencils in time and frequency domain system identification*. Developments in Control Theory Towards Glocal Control, Chapter 9. The Institution of Engineering and Technology, 2012.

[32] A. C. Ionita and A. C. Antoulas. Data-driven parametrized model reduction in the loewner framework. *SIAM Journal on Scientific Computing*, 36(3):A984–A1007, 2014.

[33] D.S. Karachalios, I.V. Gosea, and A.C. Antoulas. *Model Reduction Handbook: Volume I: System-and Data-Driven Methods and Algorithms*, chapter The Loewner Framework for System Identification and Reduction. De Gruyter, 2020.

[34] P. Kergus. *Data-driven model reference control in the frequency-domain From model reference selection to controller validation*. Ph.D. thesis, Onera, ISAE, Toulouse University, Toulouse, France, Octobre 2019.

[35] P. Kergus, C. Poussot-Vassal, F. Demourant, and S. Formentin. Frequency-domain data-driven control design in the Loewner framework. In *Proceedings of the 20th IFAC World Congress*, pages 2095–2100, Toulouse, France, July 2017.

[36] S. Lefteriu, A.C. Antoulas, and A.C. Ionita. Parametric model reduction in the loewner framework. *IFAC Proceedings Volumes*, 44(1):12751–12756, 2011. 18th IFAC World Congress.

[37] J-F. Magni. Linear fractional representation toolbox for use with matlab. Technical report, Onera, Toulouse, France, 2006.

[38] A. J. Mayo and A. C. Antoulas. A framework for the solution of the generalized realization problem. *Linear Algebra and Its Applications*, 425(2-3):634–662, 2007.

[39] D. McFarlane and K. Glover. A loop-shaping design procedure using $\mathcal{H}_\infty$ synthesis. *IEEE Transaction on Automatic Control*, 37(6):759–769, June 1992.

[40] C. Meyer, G. Broux, J. Prodigue, O. Cantinaud, and C. Poussot-Vassal. Demonstration of innovative vibration control on a Falcon Business Jet. In *Proceedings of the International Forum on Aeroelasticity and Structural Dynamics*, Como, Italy, June 2017.

[41] C. Meyer, J. Prodigue, G. Broux, O. Cantinaud, and C. Poussot-Vassal. Ground test for vibration control demonstrator. In *Proceedings of the 13th International Conference on Motion and Vibration Control*, pages 1–12, Southampton, United Kingdom, July 2016.

[42] Y. Nakatsukasa, O. Sete, and L. N. Trefethen. The AAA algorithm for rational approximation. *SIAM Journal on Scientific Computing*, 40(3):A1494–A1522, 2018.

[43] B. Peherstorfer, S. Gugercin, and K. Willcox. Data-driven reduced model construction with time-domain Loewner models. *SIAM Journal on Scientific Computing*, 39(5):A2152–A2178, 2017.

[44] C. Poussot-Vassal. *Large-scale dynamical model approximation and its applications*. HDR, habilitation thesis, Onera, INP Toulouse, Toulouse, France, July 2019.

[45] C. Poussot-Vassal, P. Kergus, F. Kerhervé, D. Sipp, and L. Cordier. Interpolatory-based data-driven pulsed fluidic actuator control design and experimental validation. *IEEE transactions on Control Systems Technology*, 2021.

[46] C. Poussot-Vassal, P. Kergus, and P. Vuillemin. , chapter Interpolation-based irrational model control design and stability analysis. to appear in Springer, 2021.

[47] C. Poussot-Vassal, C. Leclercq, and D. Sipp. Structured linear fractional parametric controller $\mathcal{H}_\infty$ design and its applications. In *Proceedings of the European Control Conference*, Limassol, Cyprus, June 2018.

[48] C. Poussot-Vassal, T. Loquen, P. Vuillemin, O. Cantinaud, and J-P. Lacoste. Business Jet Large-Scale Model Approximation and Vibration Control. In *Proceedings of the 11th IFAC ALCOSP*, pages 199–204, Caen, France, July 2013.

[49] C. Poussot-Vassal and D. Sipp. Parametric reduced order dynamical model construction of a fluid flow control problem. In *Proceedings of the 1st IFAC Workshop on Linear Parameter Varying Systems*, pages 133–138, Grenoble, France, October 2015.

[50] C. Poussot-Vassal, P. Vuillemin, O. Cantinaud, and F. Sève. Interpolatory Methods for Generic BizJet Gust Load Alleviation Function. *submitted*, 2021.

[51] D. Quero, P. Vuillemin, and C. Poussot-Vassal. A generalized eigenvalue solution to the flutter stability problem with true damping: the p-L method. *Journal of Fluids and Structures*, 103:103266, May 2021.

[52] W J. Rugh. *Nonlinear system theory - The Volterra/Wiener Approach*. The Johns Hopkins University Press, 1981.

[53] D. Sipp and P.J. Schmid. Linear Closed-Loop Control of Fluid Instabilities and Noise-Induced Perturbations: A Review of Approaches and Tools. *Applied Mechanical Revue*, 68, 2016.

[54] P. Van Dooren, K A. Gallivan, and P A. Absil. $\mathcal{H}_2$-optimal model reduction of MIMO systems. *Applied Mathematics Letters*, 21(12):53–62, December 2008.

[55] P. Vuillemin, P. Kergus, and C. Poussot-Vassal. Hybrid Loewner Data Driven Control. In *Proceedings of the IFAC World Congress*, Berlin, Germany, July 2020.

[56] K. Willcox, J. Peraire, and J White. An Arnoldi approach for generation of reduced-order models for turbomachinery. *Journal of Computers & Fluids*, 31(3):369–389, 2002.

[57] K. Zhou and J C. Doyle. *Essentials Of Robust Control*. Prentice Hall, 1997.